Cell Stem Cell

Article

PSPC1 exerts an oncogenic role in AML by regulating a leukemic transcription program in cooperation with PU.1

Graphical abstract

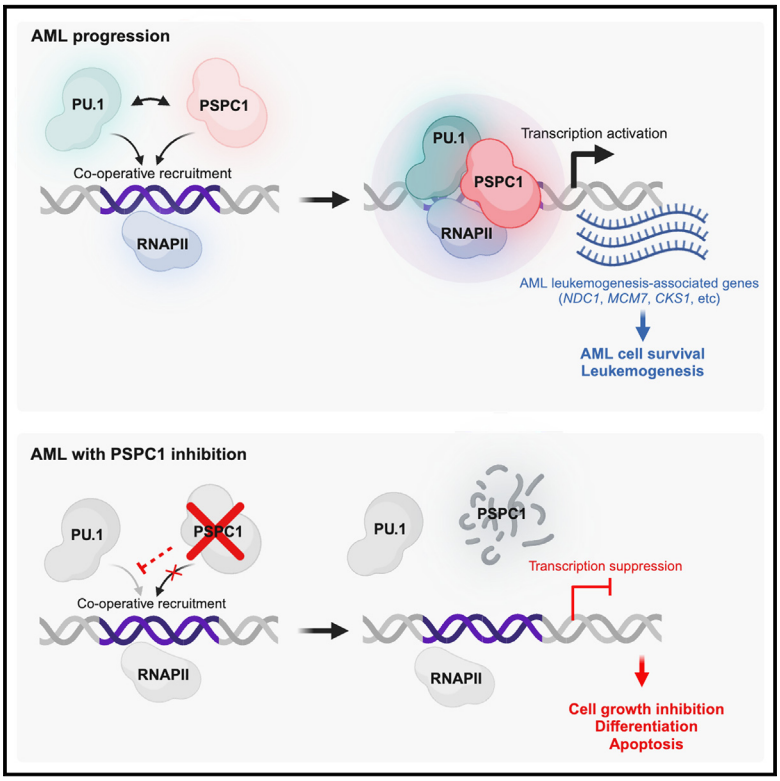

Highlights

- PSPC1 is overexpressed in AML and associated with poor prognosis in AML patients
- PSPC1 is critical for AML characteristics but dispensable for normal hematopoiesis
- PSPC1 associates with PU.1 and acts as a transcription cofactor in AML
- The PSPC1-NDC1 axis contributes to the oncogenic function of PSPC1 in AML

Authors

Juyeong Hong, Pinpin Sui, Ying Li, ..., Feng-Chun Yang, Jianlong Wang, Mingjiang Xu

Correspondence

yangf1@uthscsa.edu (F.-C.Y.), jw3925@cumc.columbia.edu (J.W.), xum1@uthscsa.edu (M.X.)

In brief

Hong et al. demonstrate that targeting PSPC1 effectively inhibits AML development/progression and self-renewal of LSCs/LICs while having little effect on normal hematopoiesis. PSPC1 interacts with PU.1 to maintain the leukemic gene transcription program in AML. These findings highlight the therapeutic potential of targeting PSPC1 to treat AML.

Hong et al., 2025, Cell Stem Cell *32*, 463–478
March 6, 2025
https://doi.org/10.1016/j.stem.2025.01.010

CellPress

Cell Stem Cell

CellPress
OPEN ACCESS

Article

PSPC1 exerts an oncogenic role in AML by regulating a leukemic transcription program in cooperation with PU.1

Juyeong Hong,[1,11] Pinpin Sui,[2,11] Ying Li,[1] Kerryn Y. Xu,[2] Ji-Hoon Lee,[1] Juan Wang,[1] Shi Chen,[1] Peng Zhang,[2] Noah Wingate,[1] Asra Noor,[2] Yaxia Yuan,[3] Robert Hromas,[4,5] Hongwei Zhou,[6] Karina Hamamoto,[7] Rui Su,[8] C. Cameron Yin,[9,10] Fengxi Ye,[9,10] Andrés E. Quesada,[9] Jianjun Chen,[8] Suming Huang,[7] Daohong Zhou,[3,5] M. James You,[9,10] Feng-Chun Yang,[2,5,*] Jianlong Wang,[6,*] and Mingjiang Xu[1,5,12,*]

[1]Department of Molecular Medicine, University of Texas Health Science Center at San Antonio, San Antonio, TX 78229, USA
[2]Department of Cell Systems & Anatomy, University of Texas Health Science Center at San Antonio, San Antonio, TX 78229, USA
[3]Department of Biochemistry & Structural Biology, University of Texas Health Science Center at San Antonio, San Antonio, TX 78229, USA
[4]Department of Medicine, University of Texas Health Science Center San Antonio, San Antonio, TX 78229, USA
[5]Mays Cancer Center, University of Texas Health Science Center at San Antonio, San Antonio, TX 78229, USA
[6]Department of Medicine, Columbia Center for Human Development and Stem Cell Therapies, Columbia University Irving Medical Center, New York, NY 10032, USA
[7]Department of Pediatrics, Pennsylvania State University College of Medicine, Hershey, PA 17033, USA
[8]Department of Systems Biology, Beckman Research Institute of City of Hope, Monrovia, CA 91016, USA
[9]Department of Hematopathology, the University of Texas MD Anderson Cancer Center, Houston, TX 77030, USA
[10]The University of Texas MD Anderson Cancer Center UT Health Houston Graduate School of Biomedical Sciences, Houston, TX 77030, USA
[11]These authors contributed equally
[12]Lead contact
*Correspondence: yangf1@uthscsa.edu (F.-C.Y.), jw3925@cumc.columbia.edu (J.W.), xum1@uthscsa.edu (M.X.)
https://doi.org/10.1016/j.stem.2025.01.010

SUMMARY

Acute myeloid leukemia (AML) is an aggressive hematopoietic malignancy characterized by the blockage of myeloid cell differentiation and uncontrolled proliferation of immature myeloid cells. Here, we show that paraspeckle component 1 (PSPC1) is aberrantly overexpressed and associated with poor survival in AML patients. Using human AML cells and mouse models, we demonstrate that PSPC1 is not required for normal hematopoiesis, but it is critical and essential for AML cells to maintain their leukemic characteristics. PSPC1 loss induces robust differentiation, suppresses proliferation, and abolishes leukemogenesis in diverse AML cells. Mechanistically, PSPC1 exerts a pro-leukemia effect by regulating a unique leukemic transcription program via cooperative chromatin binding with PU.1 and activation of tumor-promoting genes, including *NDC1*, which is not previously implicated in AML. Our findings uncover a unique and crucial role of PSPC1 dependency in AML and highlight its potential as a promising therapeutic target for AML.

INTRODUCTION

Paraspeckle component 1 (PSPC1) belongs to the *Drosophila* behavior/human splicing (DBHS) protein family, which also contains splicing factor proline/glutamine-rich (SFPQ) and non-POU domain-containing octamer-binding protein (NONO).[1,2] These DBHS proteins share highly conserved tandem N-terminal RNA-recognition motifs (RRMs), a NonA/paraspeckle domain (NOPS), and a C-terminal coiled-coil (CC) domain, which mediate direct RNA-binding, protein-protein interaction (PPI), and homo/heterodimerization among the three DBHS proteins, respectively.[1,2] Outside these conserved regions, members of the family differ significantly, both in length and sequence complexity. DBHS proteins have a nuclear localization signal at their C terminus and are largely regarded as nuclear factors, mainly localized in the nucleoplasm, paraspeckles, and chromatin.[1] Paraspeckles are composed of RNA-protein structures that include *NEAT1* and the DBHS proteins. It has been shown that SFPQ/NONO/*Neat1*, but not PSPC1, are essential components of paraspeckle formation.[3–5] Paraspeckles function in the control of gene expression via an RNA retention mechanism.[6] In addition, the domain architecture and structure of DBHS proteins have been revealed, providing insights into their homo- and heterodimerization and RNA/DNA binding modalities with biological functions.[1,2]

DBHS proteins participate in almost every step of gene regulation, including transcriptional regulation, post-transcriptional modulations of RNA stability, RNA processing and transport,

and DNA repair.[1,2] PSPC1 has been shown to modulate PRC2 functions in pluripotent stem cells to control stem cell bivalency,[7] and enhance the formation of transcription condensates to promote polymerase binding and transcription.[8] PSPC1 was also identified as one of the 15 genes located in the minimal overlapping copy number variation region of chromosome 13q12.11 in 21 cancer cell lines, including acute myeloid leukemia (AML).[9] However, studies of PSPC1 in cancer thus far have been limited to solid tumors. A study in solid tumors (breast, lung, and liver) established the functions of PSPC1 in potentiating epithelial-mesenchymal transition (EMT), stemness, and metastasis, mediated by its physical interaction with Smad2/3 to enhance transforming growth factor (TGF)-beta signaling.[9] A subsequent follow-up study on hepatocellular carcinoma further identified nonreceptor tyrosine kinase PTK6 as a PSPC1 partner, whose kinase activity phosphorylates stoichiometric PSPC1 in the nucleus, resulting in its nuclear retention as a tumor suppressor while compromising PSPC1 oncogenic functions.[10] PSPC1 overexpression causes the partner to switch from PTK6 to β-catenin, facilitating EMT, stemness, and metastasis.[10]

AML is a biologically and genetically heterogeneous hematopoietic malignancy characterized by the blockage of myeloid cell differentiation and uncontrolled proliferation of immature myeloid cells.[11–14] AML treatment has long been based on intensive chemotherapy.[15] However, unraveling the heterogeneity of AML at the clinical, cytogenetic, and molecular levels has allowed improved prognostic/predictive abilities and led to the development of selected therapies for AML subtypes with specific mutations. These include all-*trans*-retinoic acid (ATRA) and arsenic trioxide for acute promyelocytic leukemia (APL),[16] along with venetoclax (a Bcl-2 inhibitor), FLT3 inhibitors, IDH1/2 inhibitors, and others for various indications in AML.[17–24] Although treatment options for AML have been expanded over the past few decades, the 5-year overall survival of AML patients is still around 30%, according to NCI's Surveillance, Epidemiology, and End Results (SEER) program. Therefore, there remains a high unmet need to develop more effective AML therapies, which requires a deeper understanding of the pathophysiology of AML and the identification of effective molecular targets. In this study, we investigated the role of PSPC1 in normal and malignant hematopoiesis and its mechanisms of action in AML leukemogenesis.

RESULTS

PSPC1 is highly expressed in AML, and its elevated expression is correlated with poor prognosis in AML patients

We analyzed the Cancer Cell Line Encyclopedia (CCLE) database and found that AML cells expressed the highest *PSPC1* mRNA level compared with other cancer cell types (Figure 1A). This prompted us to explore the PSPC1 function in AML. NCBI Gene Expression Omnibus (GEO) datasets showed that *PSPC1* expression was significantly elevated in AML patients with different chromosomal abnormalities compared with normal controls (Figures 1B and S1A). Importantly, we observed a substantially higher level of *PSPC1* in $CD34^+$ AML cells (enriched for the leukemic stem cell [LSC] population) but not in $CD34^-$ bulk AML cells compared with normal $CD34^+$ cells (Figure S1B). In addition, we analyzed The Cancer Genome Atlas (TCGA) datasets to define high-risk and low-risk groups based on the AML patients' molecular abnormalities associated with prognosis and treatment response, which revealed that higher levels of *PSPC1* expression were found in the high-risk group compared with the low-risk group of AML patients (Figure S1C), suggesting that high expression of PSPC1 is likely associated with poor clinical outcome. Indeed, the Beat AML and TCGA cohort analyses showed that elevated *PSPC1* expression is significantly correlated with shorter survival of AML patients (Figures 1C and S1D). We also found that *PSPC1* expression levels were further enhanced at the time of relapse compared with those at diagnosis (Figure 1D), supporting the idea that high levels of *PSPC1* expression indicate poor prognosis in AML patients. To validate this observation, we assessed *PSPC1* mRNA and/or protein expression in various AML cell lines and primary AML cells, along with normal $CD34^+$ cells and mononuclear cells from bone marrow (BM) or peripheral blood (PB). We found significantly higher expression of *PSPC1* mRNA in 7 of the 8 AML cell lines (Figure 1E) and PSPC1 protein in all AML cell lines (Figure 1F) and primary patient AML cells (Figure 1G) than in normal $CD34^+$ hematopoietic stem/progenitor cells (HSPCs) and BM/PB mononuclear cells. In addition, high *PSPC1* expression was more prominent in M0, the most primitive French-American-British (FAB) subtype of AML, than in other FAB groups of AML patients (Figure S1E), suggesting that PSPC1 may be involved in AML differentiation blockage. Furthermore, the *PSPC1* expression levels were comparable across AML patients with different gene mutations, albeit slightly higher in *NPM1*-, *TP53*-, and *IDH1*-mutated groups (Figure S1F). Overall, these results indicate that PSPC1 is upregulated in pan-AML and may play a role in AML pathogenesis.

PSPC1 is essential for the maintenance of AML characteristics

The elevated expression of PSPC1 in pan-AML prompted us to investigate its roles in maintaining AML characteristics. We performed short-hairpin RNA (shRNA)-mediated knockdown and confirmed that the two independent shRNAs (shPSPC1-2 and shPSPC1-4) markedly abrogated PSPC1 expression in multiple AML cell lines (MOLM13, OCI-AML5, EOL-1, and TF-1) and primary patient AML cells (#2017-129, #2016-35, #6303, #6407, and #676) (Figures 2A, S2A, S2E, S2K, and S2M). *PSPC1* knockdown caused significant inhibition of cell growth and/or clonogenicity in MOLM13, OCI-AML5, EOL-1, TF-1, and #2017-129 AML cells (Figures 2B, 2C, S2B, and S2F). Interestingly, we found that PSPC1-depleted AML cells underwent noticeable morphological changes, including increased cell size, indented nuclei, and a decreased proportion of nucleus to cytoplasm (Figures 2D and S2C). The cell surface expression of CD11b, a myeloid differentiation marker, was also significantly increased after *PSPC1* knockdown (Figures 2D and S2C). Moreover, we observed increased erythroid differentiation in erythroleukemia TF-1 cells upon PSPC1 knockdown (Figure S2G). These results suggest that PSPC1 governs AML cell differentiation blockage. The apoptotic cell population was also increased upon *PSPC1* depletion (Figures 2E, S2D, and S2H). We further validated the effects of *PSPC1* knockdown in various AML patient cells with distinct genetic backgrounds (#2016-35, #6303, #6407, and #676) and found similar results (Figures S2I–S2N). In addition, CRISPR-Cas9-mediated *PSPC1* knockout (KO) also showed retarded cell growth and

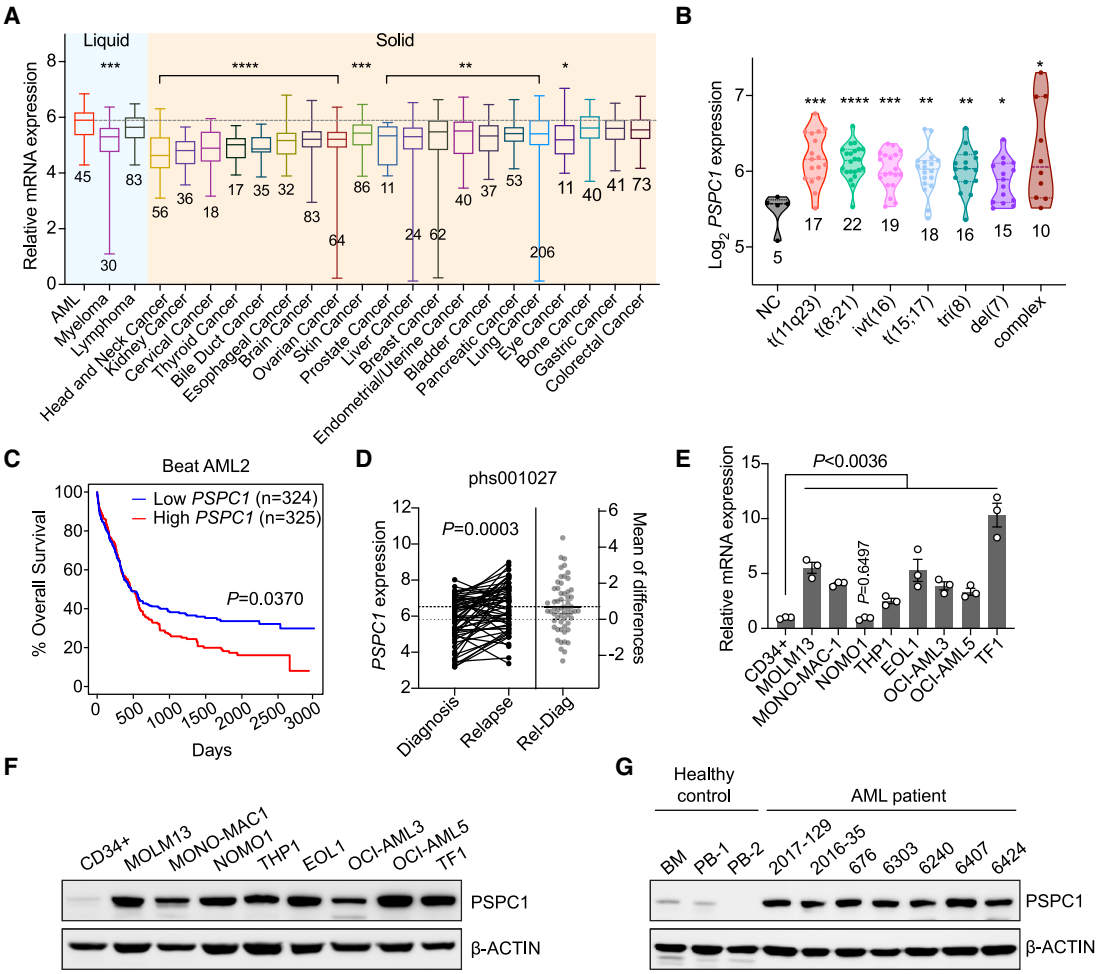

Figure 1. PSPC1 is highly expressed in AMLs and is associated with poor prognosis

(A) *PSPC1* gene expression in acute myeloid leukemia (AML) compared with other cancers from the CCLE database. Data are presented as $\log_2$ expression with range. The numbers of cell lines are shown below each bar. (*$p < 0.05$, **$p < 0.01$, ***$p < 0.001$, and ****$p < 0.0001$).

(B) Comparison of *PSPS1* expression levels in human primary AML cases with various chromosomal translocations versus healthy donors (NC) from GEO: GSE1159 datasets. The expression values were $\log_2$ transformed. The numbers of patients analyzed are presented below each bar. (*$p < 0.05$, **$p < 0.01$, ***$p < 0.001$, and ****$p < 0.0001$).

(C) Kaplan-Meier plot of overall survival in AML patients from Beat AML2 dataset. The patients were divided into two groups based on *PSPC1* expression levels. The *p* value was detected by the log-rank test.

(D) *PSPC1* gene expression at diagnosis and relapse in AML patients from phs001027 dataset.

(E and F) RT-qPCR (E) ($n = 3$) and immunoblot (F) showing PSPC1 expression in various AML cell lines and normal $CD34^+$ cells.

(G) Immunoblot showing PSPC1 expression in primary AML patient samples compared with healthy controls' PB or BM cells. Error bars denote mean ± SEM.

increased differentiation in MOLM13 and OCI-AML5 cells (Figures S2O–S2T). Collectively, these data indicate a crucial role of PSPC1 in AML progression and maintenance.

PSPC1 is critical for leukemogenesis

To further assess whether PSPC1 is required for leukemogenesis and AML progression *in vivo*, we transplanted #2017-129 or MOLM13 AML cells, transduced with GFP-expressing control shRNA (shControl) or shRNA against *PSPC1* (sh*PSPC1*), into sub-lethally irradiated immunodeficient recipient mice and monitored leukemia burden. Remarkably, mice receiving PSPC1-depleted AML cells showed significantly delayed disease development, reduced leukemia burden, and prolonged survival compared with those receiving control AML cells (Figures 3A–3C). To characterize the leukemic cells that managed to outgrow in mice receiving *PSPC1* knockdown AML cells, we first measured the GFP expression of the outgrown AML cells and found much lower levels of GFP expression in the *PSPC1* knockdown group compared with that in the control group (Figure 3D). These data indicate that a small fraction of AML cells with insufficient *PSPC1* knockdown were able to grow, leading to leukemia development. By contrast, the AML cells with sufficient knockdown lost the leukemogenic potential. To prove this, we further examined PSPC1 protein levels in $hCD45^+$ cells sorted from the terminally diseased recipient mice. We observed an equivalent abundance of PSPC1 levels

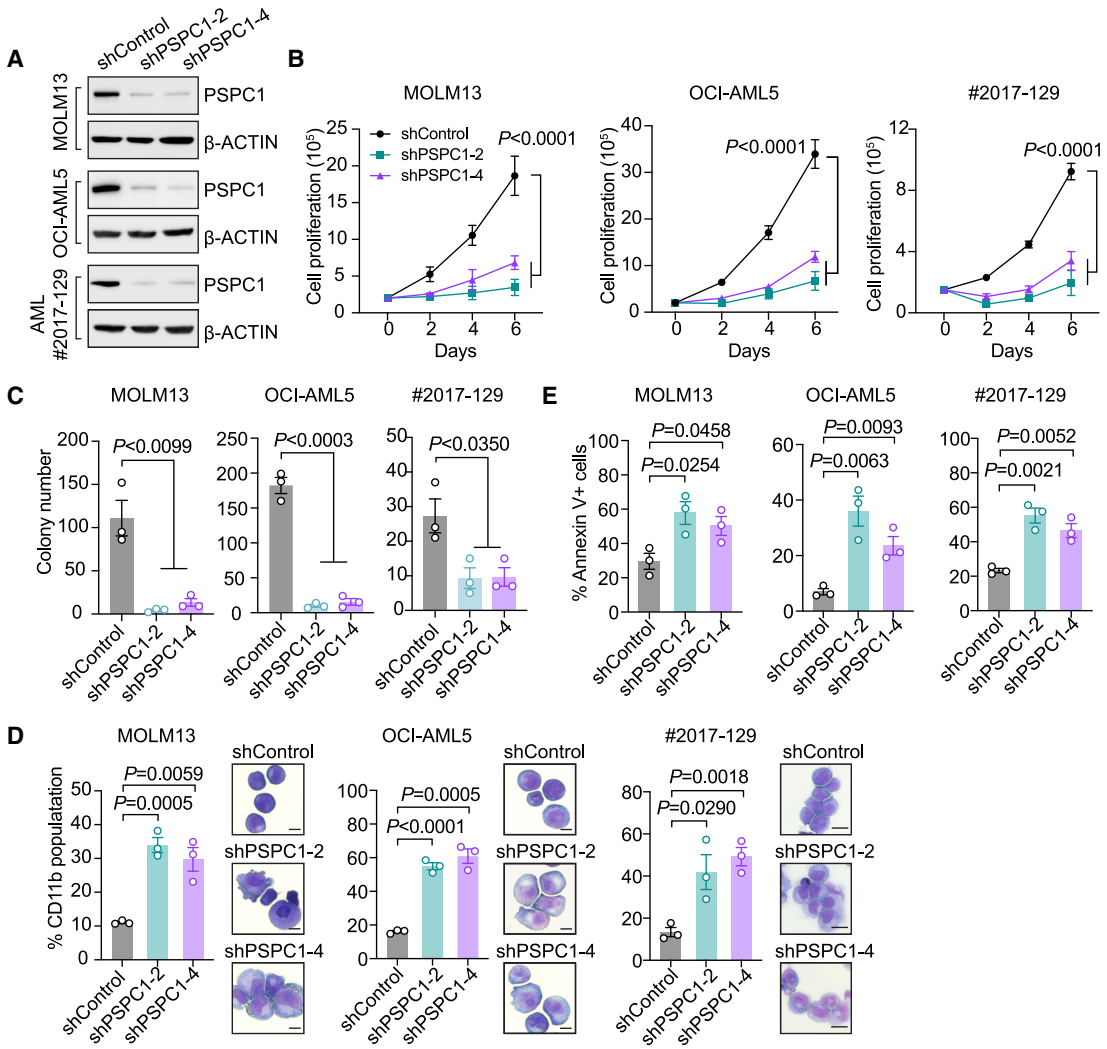

Figure 2. PSPC1 is essential for the maintenance of AML characteristics in AML cells

(A) Immunoblot showing depleted PSPC1 expression by two independent shRNA (shPSPC1-2 and shPSPC1-4) in MOLM13, OCI-AML5, and #2017-129 AML cells.

(B) Cell proliferation of shPSPC1 versus shControl expressing MOLM13, OCI-AML5, and #2017-129 AML cells (n = 3).

(C) Colony-forming unit assay from shControl or shPSPC1 MOLM13, OCI-AML5, and #2017-129 AML cells (n = 3).

(D) Flow cytometric (CD11b) and morphological analyses showing robust myeloid differentiation of MOLM13, OCI-AML5, and #2017-129 AML cells 5 days after PSPC1 depletion. Representative images of cell morphology were achieved by Wright-Giemsa staining after cytospin (n = 3). Scale bar, 10 μm.

(E) Apoptotic analysis of MOLM13, OCI-AML5, and #2017-129 AML cells 5 days after PSPC1 knockdown (n = 3). Error bars denote mean ± SEM.

in the outgrown AML cells in the PSPC1 knockdown group compared with that of the control group (Figure 3E). Similar results were obtained when #676, #2016-35, #6303, and OCI-AML5 AML cells transduced with shControl or sh*PSPC1* were transplanted (Figures S3A–S3G). The diminished *PSPC1* knockdown cell population in the recipient mice was due to their enhanced differentiation rather than altered homing capacity (Figures 3F and 3G), evidenced by dramatically increased differentiation (Figure 3G) and comparable percentages of homed MOLM13 AML cells into the BM between sh*PSPC1* and shControl groups 16 h post-transplantation (Figure 3F). Together, these data strongly suggest that *PSPC1* knockdown significantly impaired AML progression and prolonged the survival of the xenograft recipient mice, supporting the requirement of PSPC1 for maintaining human AML cell characteristics.

To address whether PSPC1 acts through paraspeckle in AML cells to mediate its pro-leukemic effects, we knocked down an essential paraspeckle component, *NONO*, in MOLM13 and OCI-AML5 cells (Figures S3H and S3L). Interestingly, NONO depletion had little effect on cell proliferation, differentiation, and apoptosis in MOLM13 and OCI-AML5 cells (Figures S3I–S3K and S3M–S3O). Moreover, consistent with previous findings,[25] *PSPC1* knockdown did not hinder paraspeckle formation in OCI-AML5 cells, while NONO depletion induced disruption of paraspeckle foci (Figures S3P–S3S). These results suggest that paraspeckle formation is not essential for key AML

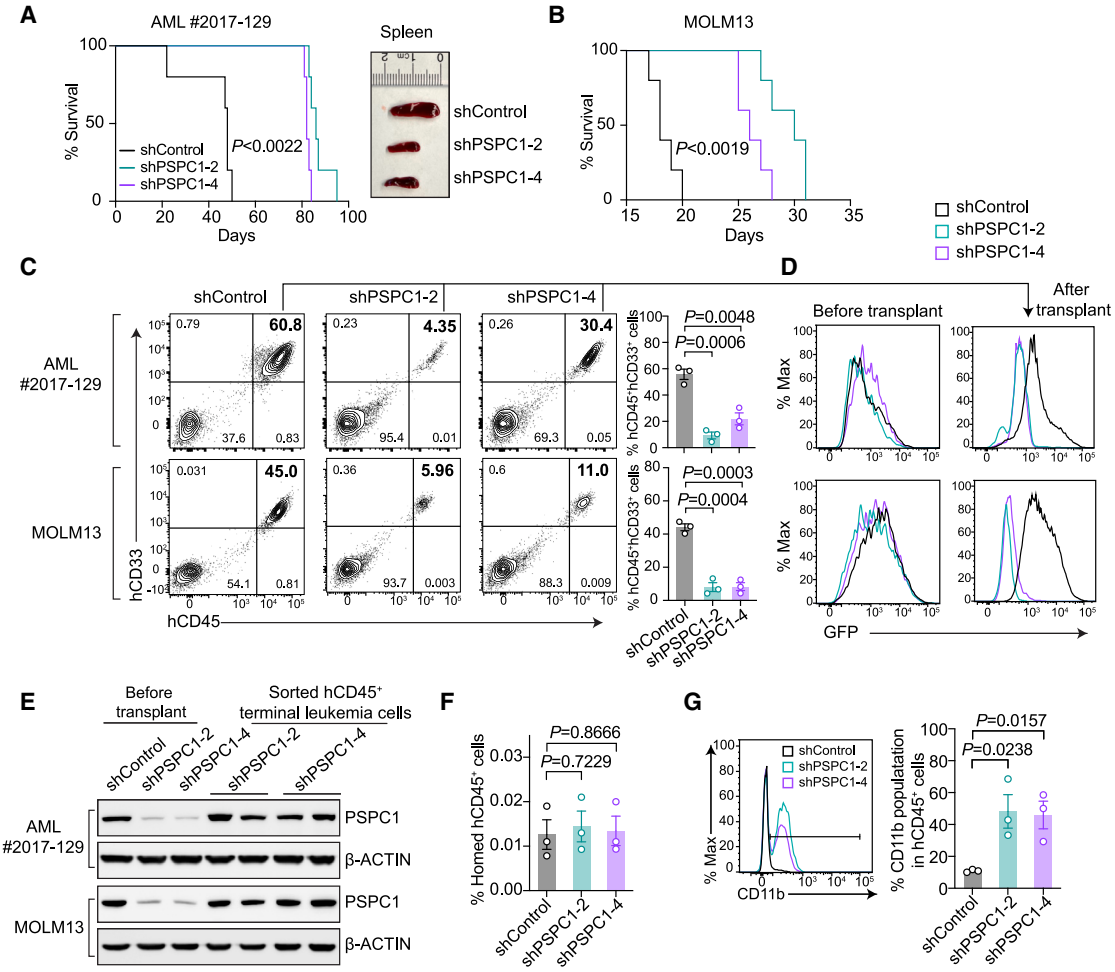

Figure 3. PSPC1 is important for AML initiation and progression *in vivo*

(A) Kaplan-Meier survival curve of NSG mice transplanted with primary #2017-129 AML cells transduced with shControl or shPSPC1 lentivirus ($n = 5$). p value was detected by the log-rank test. Representative spleen images from each group are shown (right).

(B) Kaplan-Meier survival curve of NSG mice transplanted with MOLM13 transduced with shControl or shPSPC1 lentivirus ($n = 5$). p value was detected by the log-rank test.

(C) Representative flow cytometric plot (left) of AML cell engraftment (% of human CD45 and CD33 double-positive population) in BM of recipient mice receiving primary #2017-129 AML cells (top) and MOLM13 cells (bottom). BM cells of shControl and sh*PSPC1* mice were harvested simultaneously at 45–50 days (#2017-129) and at 17–20 days (MOLM13) when a mouse in the shControl group became moribund. Quantitative summary data are shown in the right panel.

(D) Comparison of GFP expression of shControl or sh*PSPC1* transduced primary #2017-129 AML (top) and MOLM13 (bottom) AML cells before and 47 days (#2017-129) or 18 days (MOLM13) after transplantation.

(E) Immunoblot analysis of PSPC1 expression in shControl or sh*PSPC1* primary #2017-129 and MOLM13 AML cells before transplant and in sorted hCD45$^+$ cells that outgrew in moribund leukemic recipient mice.

(F and G) Flow cytometric analysis of shControl and shPSPC1 MOLM13 cells homing into BM of NSG mice (F) and their percent CD11b$^+$ cells (G). The samples were collected at 16 h post-transplantation ($n = 3$). Error bars denote mean ± SEM.

characteristics and that PSPC1 promotes AML characteristics in a paraspeckle-independent manner.

Pspc1 is required for murine AML development and progression

Leukemia stem cells (LSCs)/leukemia-initiating cells (LICs) are well-known for their roles in driving the initiation, progression, and relapse in human AML patients.[26,27] Notably, *PSPC1* expression was significantly higher in LSC-enriched than bulk AML cells in AML patients, even though *PSPC1* expression level was even lower in normal CD34$^+$ HSPCs than in normal CD34$^-$ cells (Figures S4A and S4B). These data indicate that PSPC1 may be critical for LSCs/LICs to drive leukemogenesis in AML. To elucidate the role of PSPC1 in leukemogenesis, we utilized *Pspc1*$^{f/f}$ mice[28] and crossed them with *Mx1*-Cre strain to generate *Pspc1*$^{f/f}$;*Mx1-Cre* mice in which *Pspc1* can be specifically deleted in the hematopoietic system by *pI:pC* injection (Figure 4A). The successful KO of *Pspc1* was confirmed by genotype PCR, RT-qPCR, and western blot 4 weeks after *pI:pC* injection (Figures 4B, 4C, and S4C). For simplicity, *pI:pC*-treated *Pspc1*$^{f/f}$;*Mx1-Cre* mice are referred to hereafter as *Pspc1* KO mice, and *pI:pC*-treated *Pspc1*$^{f/f}$ mice as wild-type (WT) mice.

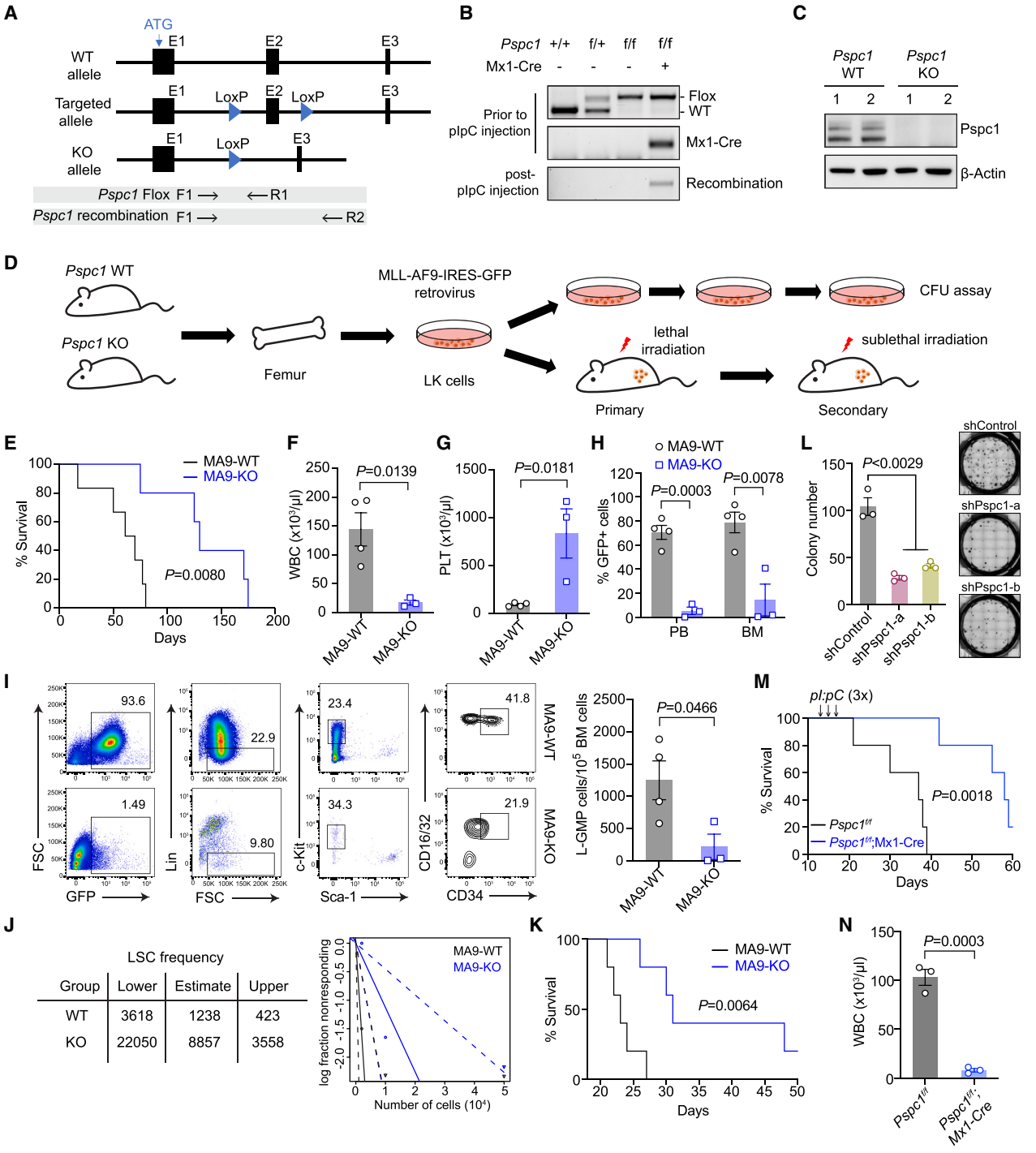

Figure 4. Pspc1 is required for MLL-AF9-mediated leukemogenesis

(A) Targeting strategy of conditional *Pspc1* KO mice.

(B and C) Representative DNA genotyping (B) and immunoblot assay (C) of BM cells from *Pspc1* WT (WT), heterozygous (f/+), or homozygous (*f/f*) mice with or without *pI:pC* injection to induce gene deletion by Cre recombination.

(D) Experimental scheme for MLL-AF9-induced mouse AML model.

(E) Kaplan-Meier survival curve of primary recipient mice transplanted with MLL-AF9 (MA9)-transduced Lin$^-$c-kit$^+$ BM cells from *Pspc1* WT and KO mice (n = 6). p value was detected by the log-rank test.

(F and G) White blood cell (WBC) (F) and platelet (PLT) (G) counts in PB of primary recipient mice (n = 3–4).

(H) Percent GFP$^+$ leukemia cells in PB and BM from primary recipient mice. PB and BM cells of MA9-WT and MA9-KO mice were harvested simultaneously at 45–80 days when a mouse in the MA9-WT group became moribund (n = 3–4).

(legend continued on next page)

We then employed MLL-AF9 (MA9)-induced cell transformation and leukemogenesis model to examine the requirement of PSPC1 in AML development since MA9 is one of the most commonly found fusion oncogenes in AML and is sufficient to drive AML without the need for another factor.[29] Lin$^-$c-Kit$^+$ (LK) BM cells from WT and *Pspc1* KO mice were transduced with MA9 (along with GFP) retrovirus and subjected to *in vitro* colony-forming unit (CFU) replating assay or *in vivo* transplantation into lethally irradiated recipient mice (Figure 4D). We found that *Pspc1* KO significantly reduced the colony numbers upon serial replating (Figure S4D). Moreover, mouse BM transplantation (BMT) assay showed that *Pspc1* abrogation significantly delayed the development of AML and prolonged the survival of MA9 recipient mice (Figure 4E). We observed that the numbers of white blood cells (WBCs) in PB and spleen size were decreased, while platelet (PLT) counts were increased in MA9-*Pspc1* KO mice compared with control MA9-*Pspc1* WT AML mice (Figures 4F, 4G, S4E, and S4F). Decreased GFP$^+$ cells in the PB, BM, and spleen, reduced immature blast cell population in PB and BM, and lower infiltration of leukemia cells in the spleen and liver were also evident in MA9-*Pspc1* KO mice compared with those in the controls (Figures 4H, S4G, and S4H). Thus, these data indicate that Pspc1 is critical for mouse AML development.

Next, we assessed the role of Pspc1 in the self-renewal of LSCs/LICs and found that the leukemic granulocyte-monocyte progenitor (L-GMP) cell population (defined as GFP$^+$Lin$^-$c-Kit$^+$Sca1$^-$CD34$^+$CD16/32$^+$) was significantly lower in the BM of primary MA9 *Pspc1* KO mice than in control MA9 WT mice (Figure 4I). To quantitatively evaluate the effect of *Pspc1* KO on LSCs/LICs frequency, we performed an *in vivo* limiting dilution assay using GFP$^+$ sorted BM cells from primary MA9 recipient mice (Figure S4I). The *Pspc1* KO group had a significantly lower LSC frequency than the control group (1:8,857 versus 1:1,238 cells) (Figure 4J) and showed prolonged survival in secondary recipient mice (Figure 4K). This was further confirmed by *in vitro* CFU assays showing that *Pspc1* knockdown in leukemic BM cells collected from MA9 primary AML mice dramatically decreased their colony-forming capacity (Figure 4L). We further asked whether *Pspc1* deletion from LSCs affects leukemia maintenance. To this end, we first induced primary leukemia by expressing MA9 in LK cells from *Pspc1*$^{f/f}$ and *Pspc1*$^{f/f}$;*Mx1-Cre* mice. GFP$^+$ sorted BM cells from primary recipient mice were transplanted into secondary recipients, and *Pspc1* deletion was induced by injecting *pI:pC* three times following leukemia engraftment (Figure S4J). Consistently, acute deletion of *Pspc1* significantly delayed the AML progression and prolonged the survival (Figure 4M). Compared with the control *Pspc1*$^{f/f}$ group, *Pspc1*$^{f/f}$;*Mx1-Cre* mice had dramatically lower WBC counts, smaller spleen size, and less liver infiltration (Figures 4N, S4K, and S4L). It is also worth noting that the infiltration of immature Gr-1$^-$Mac-1$^+$ leukemic cells in the spleen and liver was evidently lower in *Pspc1*$^{f/f}$;*Mx1-Cre* mice than that of *Pspc1*$^{f/f}$ mice (Figures S4K and S4L). Together, these data demonstrate that Pspc1 plays a critical role in maintaining the self-renewal activity of LSCs in AML.

Pspc1 is dispensable for normal hematopoiesis

To determine whether *Pspc1* deletion might cause any detrimental effect on normal hematopoiesis, we next examined the complete blood count in PB of WT and *Pspc1* KO mice 8–12 weeks after *pI:pC* injection. We found that *Pspc1* KO had no significant effect on the numbers of WBCs, lymphocytes (LYMs), granulocytes (GRAs), monocytes (MONs), platelets, and red blood cells (RBCs) (Figure 5A). In addition, the BM cellularity was similar between WT and *Pspc1* KO mice (Figure 5B). A CFU assay was performed to assess whether *Pspc1* KO affected HSPC function, and it showed comparable clonogenicity and differentiation potential between WT and *Pspc1* KO BM cells (Figure 5C). We then determined the subpopulations of HSPCs in the BM. We observed that the percentages and numbers of LSK (Lin$^-$Sca1$^+$c-Kit$^+$), LT-HSC (long-term hematopoietic stem cell), ST-HSC (short-term hematopoietic stem cell), MPP (multipotent progenitor), and LK cells in the BM of *Pspc1* KO and WT mice were similar (Figures 5D–5F and S5A). The percentages of GMP (granulocyte-macrophage progenitor), MEP (megakaryocte-erythroid progenitor), and CMP (common myeloid progenitor) populations in LK cells were also comparable (Figure 5G). Furthermore, spleen size and differentiated subpopulations, including myeloid cells (defined as Mac-1$^+$Gr-1$^+$), B cells (B220$^+$), T cells (CD4$^+$ or CD8$^+$), and erythroid cells (Ter119$^+$) in the BM, PB, and spleen were not altered by *Pspc1* depletion (Figures 5H and S5B–S5D). To further evaluate whether *Pspc1* depletion affects the repopulating capacity of HSPCs, we performed *in vivo* competitive repopulation assays. Total BM cells from *Pspc1*$^{f/f}$ or *Pspc1*$^{f/f}$;*Mx1-Cre* mice (CD45.2$^+$) were mixed with competitor BM cells (CD45.1$^+$) and transplanted into donor WT mice (CD45.1$^+$). *pI:pC* was injected 4 weeks later to ensure that *Pspc1* was deleted after transplanted cells had been completely reconstituted (Figure 5I). These chimeric mice were then monitored for 5 months after *pI:pC* injection. We found that the percentages of donor-derived total cells (CD45.2$^+$), myeloid cells, T cells, and B cells in PB were comparable between the two groups of recipient mice (Figure 5J). Consistently, no difference in the percentages of donor-derived HSC/HPC and differentiated populations was observed in the BM of WT and KO groups (Figures 5K and 5L). To further confirm that the self-renewal capacity of HSPCs is not affected by *pI:pC*, we induced *Pspc1* KO by injecting *pI:pC* into *Pspc1*$^{f/f}$ or *Pspc1*$^{f/f}$;Mx1-cre

(I) Representative flow cytometric plot and statistics showing LSC populations in the BM of primary recipient mice (n = 3–4).
(J) The limiting dilution assay. Table (left) and graph (right) show the frequency of LSCs in MA9-WT and MA9-*Pspc1* KO AML mice. The slope of the line represents the log-active cell fraction, with a steeper slope indicating a higher frequency of active cells. The "nonresponding fraction" refers to the proportion of cells that are not contained in dividing cells (n = 5 per group).
(K) Kaplan-Meier survival curve of secondary BMT recipient mice receiving an equal number of GFP$^+$ leukemia cells from primary AML mice (n = 5). p value was detected by the log-rank test.
(L) Effect of *Pspc1* knockdown on the colony-forming ability of primary MA9-WT leukemia cells.
(M) Kaplan-Meier survival curve for leukemia maintenance assay (n = 5).
(N) WBC counts in PB of recipient mice at 30–39 days when a mouse in the *Pspc1*$^{f/f}$ group became moribund (n = 3). Error bars denote mean ± SEM.

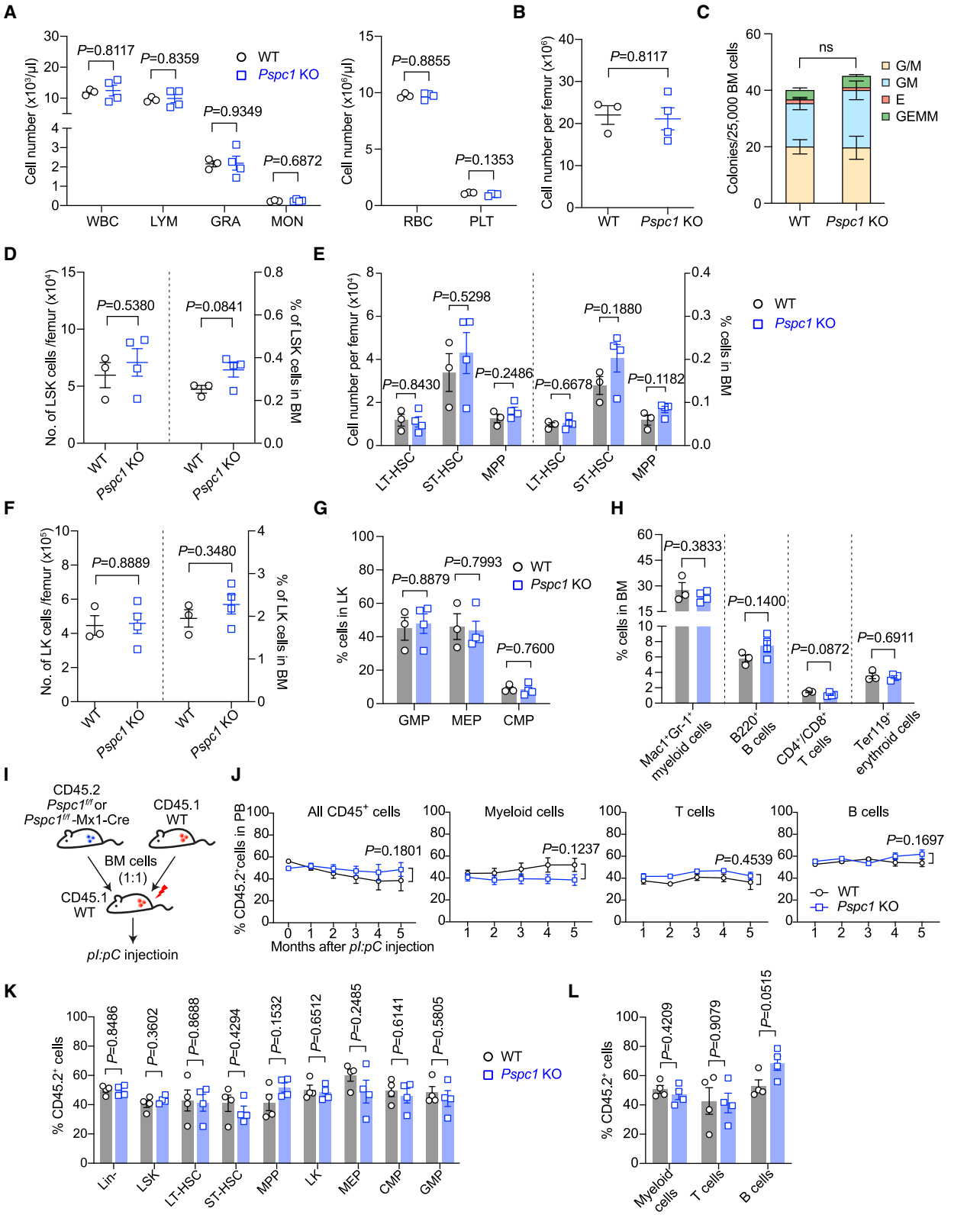

Figure 5. Pspc1 is dispensable for normal hematopoiesis and HSC function

(A) Blood counts of peripheral blood (PB) of WT and *Pspc1* KO mice at 2–3 months after *pI:pC* injection (n = 3–4).

(B) Quantitation of total bone marrow (BM) cells per femur from WT and *Pspc1* KO mice (n = 3–4).

(legend continued on next page)

mice prior to standard competitive transplantation assays using WT and *Pspc1* KO BM cells, and similar results were obtained (data not shown).

To determine whether there is a long-term effect of *Pspc1* deletion on hematopoiesis *in vivo*, we monitored the *Pspc1* KO mice for 11 months. We did not observe significant changes in any lineage of the PB or other signs of abnormal hematopoiesis in *Pspc1* KO mice (Figure S5E). Collectively, these data indicate that *Pspc1* loss is unlikely to influence normal HSPCs' function and steady-state hematopoiesis.

PSPC1 controls a unique transcription program in association with PU.1

We next sought to dissect the mechanisms by which PSPC1 exerts its oncogenic role in AML. To detect early changes, shRNA-transduced OCI-AML5 cells were selected with puromycin for 2 days and subjected to transcriptome-wide RNA sequencing (RNA-seq) analysis, which revealed 1,467 and 1,223 downregulated and upregulated genes, respectively, in OCI-AML5 cells (Figure 6A). Gene set enrichment analysis (GSEA) identified the top 10 enriched pathways in sh*PSPC1* cells compared with control cells (Figure 6B). Interestingly, *PSPC1* depletion led to significant suppression of E2F targets, G2/M checkpoints, and MYC targets. Furthermore, there was a significant decrease in the expression levels of the genes upregulated by HOXA9 and MEIS1 (Figure 6C). Additionally, Gene Ontology (GO) enrichment analysis of upregulated genes showed that myeloid differentiation was enriched in *PSPC1*-depleted cells (Figure S6A), which is consistent with our findings (Figure 2D). Similar results were obtained in MOLM13 cells following *PSPC1* knockdown (Figure S6B). Given that the expression levels of genes associated with the cell cycle were significantly downregulated by *PSPC1* depletion (Figure 6C), we performed a cell-cycle analysis. We found that *PSPC1* depletion caused an overt decrease in the proportion of cycling cells (S phase) and an increase in the proportion of cells in the G0/G1 phase in OCI-AML5, MOLM13, EOL1, and TF-1 AML cell lines (Figure S6C).

Previous studies have shown that the RNA-binding activity of PSPC1 via RRMs is important for its activity in mouse embryonic stem cells (mESCs)[8] and adipogenesis.[28] To determine whether RNA binding is critical for PSPC1's pro-leukemic role in AML, we conducted a rescue experiment by introducing shRNA-resistant PSPC1 WT and RRM deletion mutant (ΔRRM) constructs into these AML cells (Figure S6D). Expression of shRNA-resistant WT PSPC1 successfully rescued both proliferation and differentiation of OCI-AML5 AML cells with endogenous *PSPC1* knockdown. Surprisingly, ΔRRM mutant PSPC1 was also able to fully restore the reduced proliferation and enhanced myeloid differentiation associated with endogenous PSPC1 knockdown, suggesting that the RRMs of PSPC1 are not essential for its pro-leukemic function in AML (Figures S6E and S6F). Since PSPC1 has been reported to act as a transcription cofactor,[9,28] we hypothesized that PSPC1 binds to chromatin to regulate target gene transcription. We thus performed PSPC1 chromatin immunoprecipitation sequencing (ChIP-seq) in OCI-AML5 cells, identifying 7,867 peaks with most binding sites located in promoter regions (Figure 6D). Furthermore, motif analysis revealed significant enrichment of ETS transcription factor family members such as FLI1, ETV2, ETS1, GABPA, ERG1, and PU.1 in PSPC1-bound regions (Figure 6E). Among these, PU.1, but not other ETS transcription factors, was found to interact with PSPC1 in two different AML cell lines and #2017-129 AML cells by reciprocal immunoprecipitation (Figures 6F, S6G, and S6H). To determine whether PU.1 is recruited to PSPC1 binding regions, we performed PU.1 ChIP-seq in OCI-AML5 cells. Indeed, heatmap analysis of the ChIP-seq datasets revealed the co-occupancy of PU.1 with PSPC1 on the regulatory regions of PSPC1-target genes, presumably at the promoter regions (Figure 6G). Since PU.1 is a known critical transcription factor of hematopoiesis and AML,[30,31] we validated the PU.1 depletion effect in OCI-AML5 cells by demonstrating that *PU.1* knockdown significantly decreased cell proliferation (Figures 6H and S6I). Interestingly, GSEA of RNA-seq from OCI-AML5 cells upon PU.1 knockdown revealed that the enriched top 10 pathways (Figure 6I) were similar to those upon PSPC1 depletion (Figure 6B). To assess the correlation of DEGs in an unbiased manner, we analyzed all the expressed genes in *PU.1*- or *PSPC1*-depleted OCI-AML5 cells. We found that the gene expression from *PSPC1* knockdown (sh*PSPC1*) was significantly correlated with those upon *PU.1* knockdown (sh*PU.1*) (Figure 6J). Since the top 10 list mainly comprised negatively enriched pathways, we focused on the downregulated genes after *PSPC1* or *PU.1* knockdown. Indeed, GSEA showed that sh*PSPC1*-downregulated genes were also downregulated by *PU.1* knockdown, further confirming that PSPC1 and PU.1 work in the same direction (Figure S6J). We next examined whether PSPC1 and PU.1 cooperate to regulate the target gene transcription. To this end, we designed a luciferase assay using a PU.1 binding motif sequence-containing construct (Figure S6K) and transiently expressed it in OCI-AML5 cells. *PU.1* knockdown reduced the promoter activity by ~60% (Figure 6K), suggesting that the experimental setting was successful. Interestingly, *PSPC1* knockdown led to a similar decrease of the luciferase activity as *PU.1* knockdown, and combined *PSPC1* and *PU.1* knockdown further reduced the luciferase activity (Figures 6K and S6N), suggesting that PSPC1 functions as a transcriptional coactivator of PU.1. Furthermore, we performed PU.1 and PSPC1 ChIP-seq in PSPC1-depleted or PU.1-depleted OCI-AML5 cells. We confirmed that the global PSPC1 binding intensity was markedly decreased upon *PSPC1* knockdown (Figure S6M), indicating the specificity of PSPC1 signals. Notably, PU.1 recruitment to PSPC1 co-bound regions was significantly decreased after PSPC1 depletion (Figure 6L). Moreover, PSPC1 binding on

(C) CFU assay of total BM cells from WT and *Pspc1* KO mice 2 months after *pI:pC* injection ($n = 3$).
(D–H) Total cell numbers and percentages of different subpopulations of hematopoietic stem cells (D) and (E), progenitor cells (F) and (G), and differentiated cells (H) in the BM of WT and *Pspc1* KO mice 2–3 months after *pI:pC* injection ($n = 3$–4).
(I) Schematic diagram of competitive repopulation assay.
(J) Percentages of different donor-derived cell lineages in PB of recipient mice after *pI:pC* injection ($n = 4$).
(K and L) Percentages of donor-derived stem/progenitor cell (K) and differentiated cell (L) compartments in the BM of recipient mice at 5 months after *pI:pC* injection ($n = 4$). Error bars denote mean ± SEM.

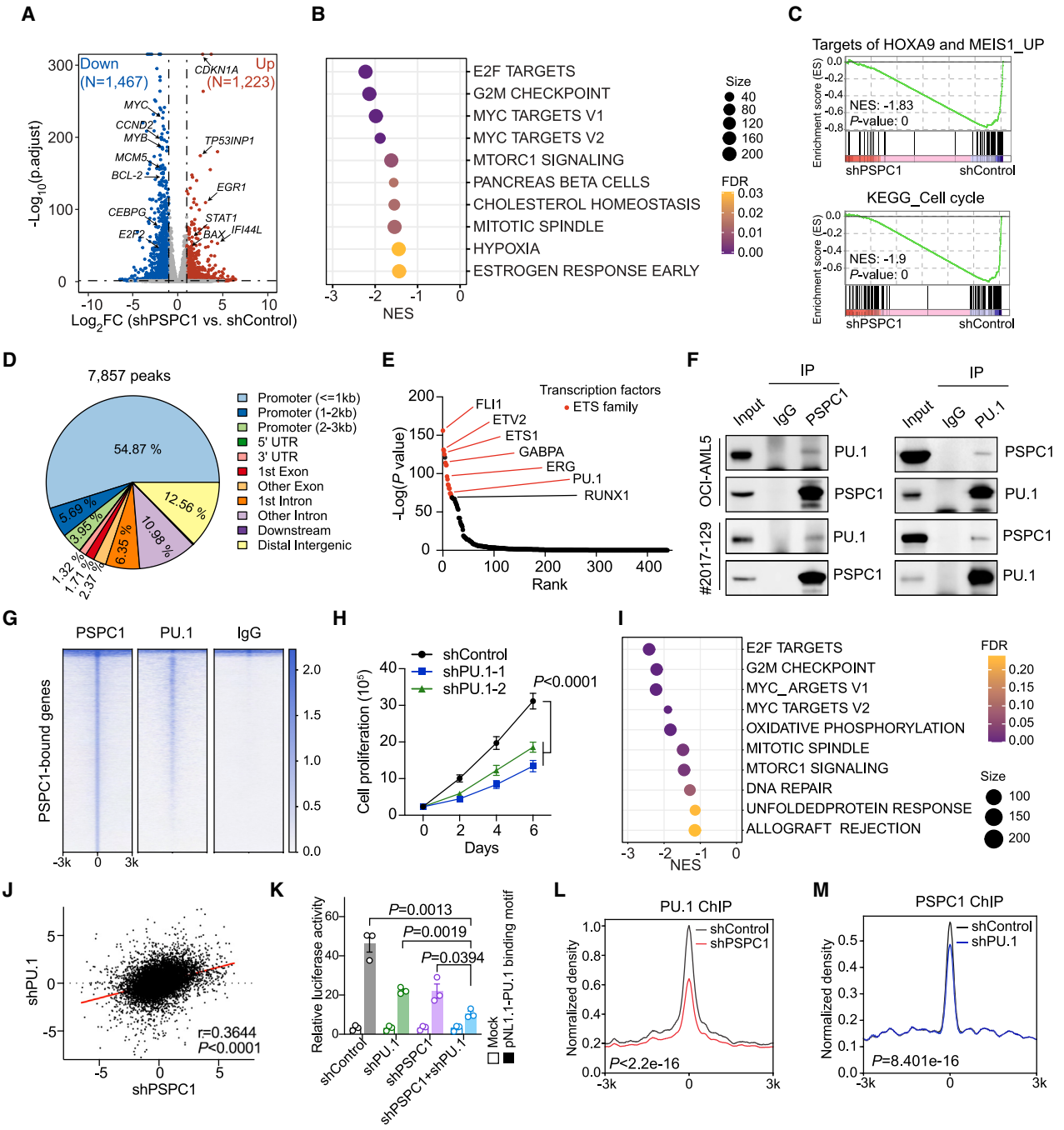

Figure 6. PSPC1 regulates target gene expression in association with PU.1 in AML cells

(A) Volcano plot showing differential gene expression upon PSPC1 depletion in OCI-AML5 cells.

(B) GSEA plot showing the top 10 significantly modulated hallmark gene sets in PSPC1-depleted (shPSPC1) OCI-AML5 cells.

(C) GSEA plots showing negative enrichment of gene sets of cell cycle and targets of HOXA9 and MEIS1 in shPSPC1 OCI-AML5 cells.

(D) Genomic distribution of PSPC1 ChIP-seq peaks.

(E) Motif analysis showing transcription factor motifs enriched in PSPC1-bound regions. Motifs of the ETS family are highlighted in red.

(F) Reciprocal co-immunoprecipitation (coIP) assay showing PSPC1 interaction with PU.1 in OCI-AML5 (top) and #2017-129 (bottom) AML cells.

(G) Heatmap of PSPC1, PU.1, and IgG ChIP-seq in PSPC1-bound regions.

(H) Cell proliferation of PU.1 knockdown (sh*PU.1*) versus control (shControl) OCI-AML5 cells (n = 3).

(I) GSEA showing the top 10 most modulated hallmark gene sets upon PU.1 depletion.

(J) Pearson's correlation of all the expressed genes in sh*PSPC1* and sh*PU.1* OCI-AML5 cells.

(legend continued on next page)

those regions was also reduced, although to a lesser extent, after PU.1 depletion (Figure 6M). These data suggest that the recruitment of PSPC1 and PU.1 on chromatin depends on each other, supporting the idea that they cooperate to regulate downstream target gene expression.

Next, we determined whether PSPC1 could promote AML characteristics in the absence of PU.1. We depleted *PSPC1* in *PU.1* knockdown OCI-AML5 cells (Figure S6N). *PU.1* loss suppressed proliferation, increased apoptosis, and induced cell-cycle arrest at the G1/S transition in OCI-AML5 cells (Figures S6O–S6Q). *PSPC1* knockdown further aggravated the effects of *PU.1* loss (Figures S6O–S6Q), suggesting that PSPC1 promotes such AML characteristics in both PU.1-dependent and -independent manners. Interestingly, the differentiation of OCI-AML5 cells was not affected by *PU.1* loss, and *PSPC1* depletion could no longer induce differentiation of OCI-AML5 cells in the absence of PU.1 (Figure S6R). These results indicate that PU.1 is required for PSPC1-mediated AML differentiation blockage in AML cells.

PSPC1 directly regulates *NDC1* transcription in AML cells

Our integrative analysis of PSPC1 and PU.1 ChIP-seq and RNA-seq datasets revealed that 96 genes were directly regulated by PSPC1 and PU.1 (Figure S7A). The major signaling pathways enriched in these 96 common target genes were analyzed, revealing the most significant enrichment of cell-cycle-associated pathways (Figure S7B). We thus validated several targets in these pathways, including *NDC1*, *MCM7*, *CDCA5*, *HAU8*, and *CKS1*, which were functionally important in various solid tumor cells and/or AML cells.[32–35] We found that both mRNA and protein expression levels of these targets were significantly reduced following PSPC1 depletion in OCI-AML5 cells (Figures S7C and S7D). *NDC1* was one of the targets showing the strongest positive correlation with *PSPC1* expression in TCGA AML dataset (Figure 7A; Table S1). In addition, high expression of *NDC1* was associated with poor survival (Figure 7B), similar to what was observed in *PSPC1* (Figure 1C). Consistent with the PU.1 and PSPC1 ChIP-seq data, our ChIP-qPCR confirmed the decreased binding of PSPC1 on *NDC1* promoter regions upon PSPC1 or PU.1 depletion as well as reduced PU.1 binding upon PSPC1 depletion (Figures 7C, 7D, S7E, and S7F). Interestingly, further analysis of TCGA dataset revealed that *NDC1* expression was significantly higher in *PSPC1*-high AML patients compared with the *PSPC1*-low group (Figure S7G). Moreover, high *NDC1* expression was correlated with poor prognosis in the *PSPC1*-high AML group but not in the low group (Figure S7H), underscoring the importance of the PSPC1-NDC1 axis in AML.

NDC1 has been reported to be overexpressed and associated with poor prognosis in various types of solid cancer (e.g., non-small lung, cervical, pancreatic, liver, and brain cancers, and sarcoma) and implicated in cell-cycle regulation and survival/proliferation in diverse solid cancer cells.[36–39] Given that such characteristics of NDC1 are similar to those of PSPC1, we further studied NDC1 function in AML cells. To assess whether *NDC1* is a functional downstream target of PSPC1, we knocked down *NDC1* in OCI-AML5 cells (Figure 7E) to examine whether *NDC1* depletion phenocopies PSPC1 loss. Notably, we observed a dramatic reduction of cell proliferation and an increase of apoptosis in *NDC1*-depleted OCI-AML5 cells (Figures 7F and 7G), which recapitulated the phenotypes resulting from *PSPC1* depletion (Figures 2B and 2E). Moreover, cell-cycle analysis showed that cells in the G0/G1 phase significantly increased while those in the S phase decreased upon *NDC1* depletion (Figure 7H), which is also consistent with the effects of PSPC1 depletion (Figure S6C). However, unlike PSPC1 loss, we did not observe changes in myeloid differentiation following *NDC1* depletion (Figure S7I), suggesting additional target genes are involved in PSPC1-mediated differentiation blockage in AML cells. Next, we examined whether NDC1 overexpression could rescue any of the phenotypes of PSPC1 knockdown AML cells by overexpressing NDC1 in *PSPC1* knockdown OCI-AML5 cells (Figure 7I). Forced expression of NDC1 partially yet significantly restored *PSPC1* knockdown-induced AML cell proliferation defects, cell-cycle arrest, and apoptosis, but not differentiation (Figures 7J–7M). These results indicate that NDC1 is a functionally important target of PSPC1 and partly contributes to PSPC1's pro-leukemic effects in AML cells.

DISCUSSION

It has been reported that PSPC1 promotes stemness and metastasis in solid tumors by serving as the molecular switch for TGF-beta[9,40] and PTK6.[10,41] In this study, we investigated the role of PSPC1 in AML, which led to the following significant findings. First, PSPC1 is highly overexpressed in virtually all types of human AMLs. Second, *PSPC1* knockdown profoundly suppresses proliferation, promotes apoptosis, induces robust differentiation of diverse AML cells, and abrogates their leukemogenic capacity in xeno-transplanted recipient mice. Third, using inducible *Pspc1* KO mice, we found that *Pspc1* deletion has little effect on HSPC function and steady-state hematopoiesis. Fourth, despite being a member of the DBHS protein family associated with nuclear paraspeckles that also contain SFPQ and NONO,[1] neither paraspeckles nor NONO is involved in PSPC1-mediated hyperproliferation and myeloid differentiation arrest in AML cells. Fifth, integrated PSPC1 ChIP-seq and RNA-seq analyses in WT versus *PSPC1* knockdown AML cells identified key target genes important for oncogenesis, proliferation, and survival of AML cells, including *NDC1*, previously unappreciated in AML. Motif and candidate approach analyses revealed putative transcription factors, such as PU.1, cooperating with PSPC1 to regulate their common target gene

(K) Bar graph showing relative luciferase activity in *PU.1* or/and *PSPC1* knockdown OCI-AML5 cells normalized to firefly luciferase in control OCI-AML5 cells. OCI-AML5 cells were transfected with luciferase reporter vectors (pNL1.1-vector and pTK-firefly), and luciferase activity was detected by a nano-glo dual luciferase assay system ($n = 3$).
(L) PU.1 ChIP-seq density plot showing decreased PU.1-bound intensity in PSPC1 knockdown OCI-AML5 cells compared with shControl cells.
(M) PSPC1 ChIP-seq density plot showing decreased PSPC1-bound intensity in PU.1 knockdown OCI-AML5 cells compared with shControl cells.
p value was detected by the paired t tests for (L) and (M). Error bars denote mean ± SEM.

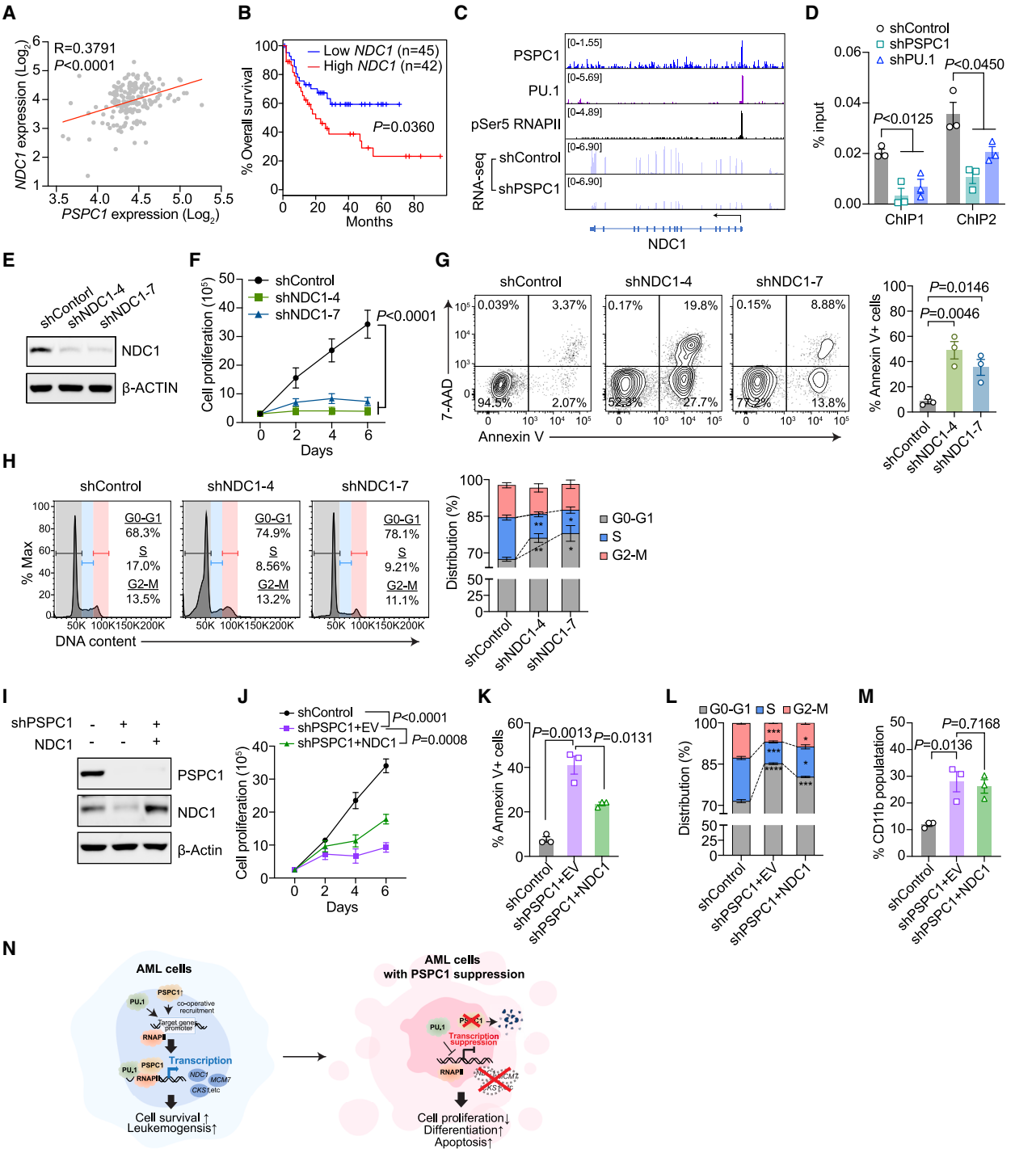

Figure 7. *NDC1* is a functionally important target of PSPC1 in AML

(A) Pearson's correlation of *PSPC1* and *NDC1* mRNA levels in TCGA AML dataset.

(B) Kaplan-Meier plot of overall survival in AML patients from TCGA dataset. The patients were divided into two groups based on *NDC1* expression levels. *p* value was detected by the log-rank test.

(C) Integrative Genomic Viewer (IGV) browser view of PSPC1, PU.1, and pSer5 RNA polymerase II (RNAPII) ChIP-seq at *NDC1* promoter in OCI-AML5 cells and RNA abundance of *NDC1* transcripts detected by RNA-seq in PSPC1 knockdown or control OCI-AML5 cells.

(D) ChIP-qPCR analysis showing PSPC1 binding to *NDC1* promoter regions (ChIP1 and ChIP2) in OCI-AML 5 cells upon PSPC1 or PU.1 depletion ($n = 3$).

(E) Immunoblot of NDC1 expression post-transduction with two different *NDC1* shRNAs in OCI-AML5 cells.

(F) Cell proliferation of OCI-AML5 cells upon NDC1 depletion ($n = 3$).

(legend continued on next page)

expression. These findings, summarized in the model (Figure 7N), establish PSPC1 as a potent determinant for key characteristics of AML via a mechanistic action distinct from solid tumors, offering a potential therapeutic strategy for AMLs by PSPC1 inhibition.

Despite the recent development and ever-increasing options of AML-directed therapies, most leukemia-associated mutations are not yet actionable.[42] Although the multiple subtypes in AML may require very different therapies, it is critical to discover common dependencies for AMLs driven by diverse drivers. Targeted therapies based on such unique dependency would serve as a "one-size-fits-all" therapy for numerous AML subtypes, as they will be effective toward diverse AML cells, including the ones harboring multiple driver mutations. Given our observed uniform anti-leukemic effects of PSPC1 inhibition in numerous AML cell lines and primary AML cells, and the similar anti-leukemic effects of PSPC1 inhibition in AMLs driven by classic drivers such as *MLL-AF9*, PSPC1 is likely a common dependency for AMLs driven by diverse drivers, and PSPC1 inhibition could be a promising therapeutic strategy across various AML subtypes.

Developing an effective therapeutic strategy targeting PSPC1 for AMLs requires a deeper understanding of the molecular mechanisms by which PSPC1 promotes AML. As a member of the DBHS protein family, PSPC1 is mainly localized in the nucleoplasm, paraspeckles, and chromatin. Our earlier studies in mESCs revealed RNA-binding functions of PSPC1 in mediating chromatin targeting of TET2 for endogenous retrovirus control in pluripotent stem cells,[43] modulating PRC2 functions via a TET1-PSPC1-Neat1 molecular axis to control stem cell bivalency,[7] and enhancing the formation of transcription condensates to promote polymerase binding and transcription.[8] While exploring its potential roles in leukemogenesis, we found by surprise that neither paraspeckles/NONO nor RNA-binding domain of PSPC1 is essential for the pro-leukemic roles of PSPC1 in AML cells. Previous studies reported that long non-coding RNA *Neat1* regulates AML in a paraspeckle-independent manner, suggesting that paraspeckle components have a distinct function beyond paraspeckle assembly.[44,45] Our integrated analysis of ChIP-seq and RNA-seq datasets further identified direct PSPC1-activated and -repressed transcriptional target genes with leukemic and tumor-suppressive functions, respectively, and notable enrichment of binding motifs for ETS family proteins with well-established roles in leukemia.[46] This raises the possibility of a link between PSPC1 and ETS transcription factors for transcriptional regulation in AML. Based on our findings of PSPC1 in AML cells, PSPC1 and its interacting partner PU.1 regulate critical downstream leukemic and tumor-suppressive genes for transcriptional activation and repression, respectively. Furthermore, our PSPC1/PU.1 common target gene analysis identified downstream functional important genes previously unappreciated in leukemogenesis, such as *NDC1*. Our studies on NDC1 revealed its roles in PSPC1-mediated regulation of proliferation, cell cycle, and apoptosis in AML cells. These findings provide valuable insights into the development of PSPC1 inhibitors for improved therapeutics of not only AML but also numerous solid cancers where PSPC1 stimulates metastasis.[9,10]

PSPC1 is highly overexpressed in various subtypes of AML (Figure 1). It is thus important to determine whether PSPC1 overexpression alone can perturb HSPC function and lead to leukemic transformation without other AML drivers. Forced expression of *Pspc1* in mouse LK cells did not show altered colony-forming and replating capacity *in vitro* (Figure S7J), suggesting that PSPC1 overexpression is likely not oncogenic per se but instead plays a critical and essential role in maintaining AML cell characteristics driven by diverse AML drivers. Nevertheless, our studies demonstrate that PSPC1 is an ideal, safe, and effective therapeutic target in various AML subtypes.

Limitations of the study

Although *Pspc1* KO significantly prolonged survival in the MA9-AML model, it is noteworthy that longer-latency leukemias could still develop in our *Pspc1* KO MLL model (Figure 4E), which had undetectable Pspc1 expression (Figure S7K). This eventual AML development could be due to a gained leukemogenic pathway bypassing/replacing Pspc1. Future investigation is warranted to assess how these AMLs develop resistance to Pspc1 depletion long-term *in vivo*.

RESOURCE AVAILABILITY

Lead contact

Further information and requests for reagents should be directed to and will be fulfilled by the lead contact, Mingjiang Xu (xum1@uthscsa.edu).

Materials availability

All the materials generated in this manuscript are available from the lead contact under a complete Materials Transfer Agreement.

Data and code availability

- RNA-seq and ChIP-seq data generated in this study have been deposited in the gene expression omnibus (GEO) and made accessible under accession number GEO: GSE247302.
- This paper does not report original code.
- Any additional information required to reanalyze the data reported in this paper is available from the lead contact upon request.

ACKNOWLEDGMENTS

We thank Dr. P. Tontonoz at UCLA for providing the mouse sperm with the *Pspc1 flox* allele. Funding: this work is supported by the National Institute of

(G) Representative plot (left) and quantitative summary (right) of apoptotic analysis of OCI-AML5 cells 4 days after NDC1 knockdown ($n = 3$).
(H) Representative plot (left) and quantitative summary (right) of cell-cycle analysis of OCI-AML5 cells upon NDC1 depletion by staining with propidium iodide (PI) ($n = 3$).
(I) Immunoblot showing NDC1 and PSPC1 protein expression in OCI-AML5 cells with or without PSPC1 knockdown, together with the expression of an empty or NDC1-encoding vector as indicated.
(J–M) Cell proliferation (J), apoptosis (K), cell cycle (L), and myeloid differentiation (M) of OCI-AML5 cells with or without PSPC1 knockdown and/or NDC1 overexpression ($n = 3$).
(N) Working model showing the role of PSPC1 in the regulation of leukemic gene transcription and characteristics of AML cells. Error bars denote mean ± SEM.

Health (NIH) HL146664 and CA285299 to M.X. and Jianlong Wang, HL174477 to M.X., CA260729 to M.X. and S.H., and CA172408 to M.X. and F.-C.Y. The research in the Wang (Jianlong Wang) laboratory is also supported by NIH (HD095938, HD097268, and BC200469). M.J.Y. and Y.Y. are partially funded by the Institutional Research Grant from the University of Texas MD Anderson Cancer Center.

AUTHOR CONTRIBUTIONS

M.X. supervised the entire project. M.X. and J.H. conceived the original idea and designed the initial studies with input from Jianlong Wang and F.-C.Y. J.H. performed most cell studies with the help of Y.L., J.-H.L., Juan Wang, N.W., A.N., and S.C. P.S. and K.Y.X. performed bioinformatics analysis and interpreted the data with the input from F.-C.Y. Under the supervision of M.X. and F.-C.Y., J.H., Y.L., Juan Wang, K.H., R.S., H.Z., and P.Z. performed *in vivo* studies with mice and primary cells. C.C.Y., F.Y., A.E.Q., M.J.Y., and J.C. provided AML samples for the study. M.X., J.H., Jianlong Wang, and F.-C.Y. wrote the manuscript with input from Y.Y., R.H., J.C., S.H., D.Z., and M.J.Y. All authors approved the final manuscript.

DECLARATION OF INTERESTS

The authors declare no competing interests.

STAR★METHODS

Detailed methods are provided in the online version of this paper and include the following:

- KEY RESOURCES TABLE
- EXPERIMENTAL MODEL AND STUDY PARTICIPANT DETAILS
  - Human patient samples and primary cell culture
  - Mice
  - Cell lines
- METHOD DETAILS
  - Plasmids
  - Lentivirus production and generation of stable cell lines
  - Retrovirus preparation and *in vitro* colony-forming assay
  - Bone marrow transplantation (BMT)
  - Competitive repopulation assay
  - Xenotransplantation assay
  - *In vivo* homing assay
  - Flow cytometry
  - Western blots and co-immunoprecipitation (co-IP) assay
  - Immunofluorescence (IF) assay
  - Luciferase assay
  - RNA extraction and quantitative reverse transcription PCR (RT-qPCR)
  - RNA-seq and data analysis
  - Chromatin immunoprecipitation (ChIP)-qPCR and ChIP-seq
- QUANTIFICATION AND STATISTICAL ANALYSIS

SUPPLEMENTAL INFORMATION

Supplemental information can be found online at https://doi.org/10.1016/j.stem.2025.01.010.

Received: December 28, 2023
Revised: November 1, 2024
Accepted: January 16, 2025
Published: February 14, 2025

REFERENCES

1. Knott, G.J., Bond, C.S., and Fox, A.H. (2016). The DBHS proteins SFPQ, NONO and PSPC1: a multipurpose molecular scaffold. Nucleic Acids Res. *44*, 3989–4004. https://doi.org/10.1093/nar/gkw271.
2. Knott, G.J., Chong, Y.S., Passon, D.M., Liang, X.H., Deplazes, E., Conte, M.R., Marshall, A.C., Lee, M., Fox, A.H., and Bond, C.S. (2022). Structural basis of dimerization and nucleic acid binding of human DBHS proteins NONO and PSPC1. Nucleic Acids Res. *50*, 522–535. https://doi.org/10.1093/nar/gkab1216.
3. Naganuma, T., Nakagawa, S., Tanigawa, A., Sasaki, Y.F., Goshima, N., and Hirose, T. (2012). Alternative 3′-end processing of long noncoding RNA initiates construction of nuclear paraspeckles. EMBO J. *31*, 4020–4034. https://doi.org/10.1038/emboj.2012.251.
4. Fox, A.H., Bond, C.S., and Lamond, A.I. (2005). P54nrb forms a heterodimer with PSP1 that localizes to paraspeckles in an RNA-dependent manner. Mol. Biol. Cell *16*, 5304–5315. https://doi.org/10.1091/mbc.E05-06-0587.
5. Fox, A.H., Nakagawa, S., Hirose, T., and Bond, C.S. (2018). Paraspeckles: where long noncoding RNA meets phase separation. Trends Biochem. Sci. *43*, 124–135. https://doi.org/10.1016/j.tibs.2017.12.001.
6. Wang, Y., and Chen, L.L. (2020). Organization and function of paraspeckles. Essays Biochem. *64*, 875–882. https://doi.org/10.1042/EBC20200010.
7. Huang, X., Bashkenova, N., Hong, Y., Lyu, C., Guallar, D., Hu, Z., Malik, V., Li, D., Wang, H., Shen, X., et al. (2022). A TET1-PSPC1-Neat1 molecular axis modulates PRC2 functions in controlling stem cell bivalency. Cell Rep. *39*, 110928. https://doi.org/10.1016/j.celrep.2022.110928.
8. Shao, W., Bi, X., Pan, Y., Gao, B., Wu, J., Yin, Y., Liu, Z., Peng, M., Zhang, W., Jiang, X., et al. (2022). Phase separation of RNA-binding protein promotes polymerase binding and transcription. Nat. Chem. Biol. *18*, 70–80. https://doi.org/10.1038/s41589-021-00904-5.
9. Yeh, H.W., Hsu, E.C., Lee, S.S., Lang, Y.D., Lin, Y.C., Chang, C.Y., Lee, S.Y., Gu, D.L., Shih, J.H., Ho, C.M., et al. (2018). PSPC1 mediates TGF-beta1 autocrine signalling and Smad2/3 target switching to promote EMT, stemness and metastasis. Nat. Cell Biol. *20*, 479–491. https://doi.org/10.1038/s41556-018-0062-y.
10. Lang, Y.D., Chen, H.Y., Ho, C.M., Shih, J.H., Hsu, E.C., Shen, R., Lee, Y.C., Chen, J.W., Wu, C.Y., Yeh, H.W., et al. (2019). PSPC1-interchanged interactions with PTK6 and beta-catenin synergize oncogenic subcellular translocations and tumor progression. Nat. Commun. *10*, 5716. https://doi.org/10.1038/s41467-019-13665-6.
11. Löwenberg, B., and Rowe, J.M. (2016). Introduction to the review series on advances in acute myeloid leukemia (AML). Blood *127*, 1. https://doi.org/10.1182/blood-2015-10-662684.
12. Khwaja, A., Bjorkholm, M., Gale, R.E., Levine, R.L., Jordan, C.T., Ehninger, G., Bloomfield, C.D., Estey, E., Burnett, A., Cornelissen, J.J., et al. (2016). Acute myeloid leukaemia. Nat. Rev. Dis. Primers *2*, 16010. https://doi.org/10.1038/nrdp.2016.10.
13. Li, S., Mason, C.E., and Melnick, A. (2016). Genetic and epigenetic heterogeneity in acute myeloid leukemia. Curr. Opin. Genet. Dev. *36*, 100–106. https://doi.org/10.1016/j.gde.2016.03.011.
14. Zeng, A.G.X., Bansal, S., Jin, L., Mitchell, A., Chen, W.C., Abbas, H.A., Chan-Seng-Yue, M., Voisin, V., van Galen, P., Tierens, A., et al. (2022). A cellular hierarchy framework for understanding heterogeneity and predicting drug response in acute myeloid leukemia. Nat. Med. *28*, 1212–1223. https://doi.org/10.1038/s41591-022-01819-x.
15. Dombret, H., and Gardin, C. (2016). An update of current treatments for adult acute myeloid leukemia. Blood *127*, 53–61. https://doi.org/10.1182/blood-2015-08-604520.
16. Lo-Coco, F., Avvisati, G., Vignetti, M., Thiede, C., Orlando, S.M., Iacobelli, S., Ferrara, F., Fazi, P., Cicconi, L., Di Bona, E., et al. (2013). Retinoic acid and arsenic trioxide for acute promyelocytic leukemia. N. Engl. J. Med. *369*, 111–121. https://doi.org/10.1056/NEJMoa1300874.
17. DiNardo, C.D., Jonas, B.A., Pullarkat, V., Thirman, M.J., Garcia, J.S., Wei, A.H., Konopleva, M., Döhner, H., Letai, A., Fenaux, P., et al. (2020). Azacitidine and venetoclax in previously untreated acute myeloid leukemia. N. Engl. J. Med. *383*, 617–629. https://doi.org/10.1056/NEJMoa2012971.

18. Wei, A.H., Montesinos, P., Ivanov, V., DiNardo, C.D., Novak, J., Laribi, K., Kim, I., Stevens, D.A., Fiedler, W., Pagoni, M., et al. (2020). Venetoclax plus LDAC for newly diagnosed AML ineligible for intensive chemotherapy: a phase 3 randomized placebo-controlled trial. Blood *135*, 2137–2145. https://doi.org/10.1182/blood.2020004856.

19. Roboz, G.J., DiNardo, C.D., Stein, E.M., de Botton, S., Mims, A.S., Prince, G.T., Altman, J.K., Arellano, M.L., Donnellan, W., Erba, H.P., et al. (2020). Ivosidenib induces deep durable remissions in patients with newly diagnosed IDH1-mutant acute myeloid leukemia. Blood *135*, 463–471. https://doi.org/10.1182/blood.2019002140.

20. DiNardo, C.D. (2018). Ivosidenib in IDH1-mutated acute myeloid leukemia. N. Engl. J. Med. *379*, 1186. https://doi.org/10.1056/NEJMc1809507.

21. Stein, E.M., DiNardo, C.D., Pollyea, D.A., Fathi, A.T., Roboz, G.J., Altman, J.K., Stone, R.M., DeAngelo, D.J., Levine, R.L., Flinn, I.W., et al. (2017). Enasidenib in mutant IDH2 relapsed or refractory acute myeloid leukemia. Blood *130*, 722–731. https://doi.org/10.1182/blood-2017-04-779405.

22. Perl, A.E., Martinelli, G., Cortes, J.E., Neubauer, A., Berman, E., Paolini, S., Montesinos, P., Baer, M.R., Larson, R.A., Ustun, C., et al. (2019). Gilteritinib or chemotherapy for relapsed or refractory FLT3-mutated AML. N. Engl. J. Med. *381*, 1728–1740. https://doi.org/10.1056/NEJMoa1902688.

23. Cortes, J.E., Khaled, S., Martinelli, G., Perl, A.E., Ganguly, S., Russell, N., Krämer, A., Dombret, H., Hogge, D., Jonas, B.A., et al. (2019). Quizartinib versus salvage chemotherapy in relapsed or refractory FLT3-ITD acute myeloid leukaemia (QuANTUM-R): a multicentre, randomised, controlled, open-label, phase 3 trial. Lancet Oncol. *20*, 984–997. https://doi.org/10.1016/S1470-2045(19)30150-0.

24. Stone, R.M., Mandrekar, S.J., Sanford, B.L., Laumann, K., Geyer, S., Bloomfield, C.D., Thiede, C., Prior, T.W., Döhner, K., Marcucci, G., et al. (2017). Midostaurin plus chemotherapy for acute myeloid leukemia with a FLT3 mutation. N. Engl. J. Med. *377*, 454–464. https://doi.org/10.1056/NEJMoa1614359.

25. Sasaki, Y.T.F., Ideue, T., Sano, M., Mituyama, T., and Hirose, T. (2009). MENepsilon/beta noncoding RNAs are essential for structural integrity of nuclear paraspeckles. Proc. Natl. Acad. Sci. USA *106*, 2525–2530. https://doi.org/10.1073/pnas.0807899106.

26. Hope, K.J., Jin, L., and Dick, J.E. (2004). Acute myeloid leukemia originates from a hierarchy of leukemic stem cell classes that differ in self-renewal capacity. Nat. Immunol. *5*, 738–743. https://doi.org/10.1038/ni1080.

27. Shlush, L.I., Mitchell, A., Heisler, L., Abelson, S., Ng, S.W.K., Trotman-Grant, A., Medeiros, J.J.F., Rao-Bhatia, A., Jaciw-Zurakowsky, I., Marke, R., et al. (2017). Tracing the origins of relapse in acute myeloid leukaemia to stem cells. Nature *547*, 104–108. https://doi.org/10.1038/nature22993.

28. Wang, J., Rajbhandari, P., Damianov, A., Han, A., Sallam, T., Waki, H., Villanueva, C.J., Lee, S.D., Nielsen, R., Mandrup, S., et al. (2017). RNA-binding protein PSPC1 promotes the differentiation-dependent nuclear export of adipocyte RNAs. J. Clin. Invest. *127*, 987–1004. https://doi.org/10.1172/JCI89484.

29. Corral, J., Lavenir, I., Impey, H., Warren, A.J., Forster, A., Larson, T.A., Bell, S., McKenzie, A.N., King, G., and Rabbitts, T.H. (1996). An Mll-AF9 fusion gene made by homologous recombination causes acute leukemia in chimeric mice: a method to create fusion oncogenes. Cell *85*, 853–861. https://doi.org/10.1016/s0092-8674(00)81269-6.

30. Antony-Debré, I., Paul, A., Leite, J., Mitchell, K., Kim, H.M., Carvajal, L.A., Todorova, T.I., Huang, K., Kumar, A., Farahat, A.A., et al. (2017). Pharmacological inhibition of the transcription factor PU.1 in leukemia. J. Clin. Invest. *127*, 4297–4313. https://doi.org/10.1172/JCI92504.

31. Curtiss, B.M., VanCampen, J., Macaraeg, J., Kong, G.L., Taherinasab, A., Tsuchiya, M., Yashar, W.M., Tsang, Y.H., Horton, W., Coleman, D.J., et al. (2022). PU.1 and MYC transcriptional network defines synergistic drug responses to KIT and LSD1 inhibition in acute myeloid leukemia. Leukemia *36*, 1781–1793. https://doi.org/10.1038/s41375-022-01594-1.

32. Qu, K., Wang, Z., Fan, H., Li, J., Liu, J., Li, P., Liang, Z., An, H., Jiang, Y., Lin, Q., et al. (2017). MCM7 promotes cancer progression through cyclin D1-dependent signaling and serves as a prognostic marker for patients with hepatocellular carcinoma. Cell Death Dis. *8*, e2603. https://doi.org/10.1038/cddis.2016.352.

33. Shen, A., Liu, L., Chen, H., Qi, F., Huang, Y., Lin, J., Sferra, T.J., Sankararaman, S., Wei, L., Chu, J., et al. (2019). Cell division cycle associated 5 promotes colorectal cancer progression by activating the ERK signaling pathway. Oncogenesis *8*, 19. https://doi.org/10.1038/s41389-019-0123-5.

34. Wang, T., Yao, S., Li, S., Fei, X., and Zhang, M. (2023). A prognostic model based on the Augmin family genes for LGG patients. Sci. Rep. *13*, 7520. https://doi.org/10.1038/s41598-023-34779-4.

35. Grey, W., Rio-Machin, A., Casado, P., Grönroos, E., Ali, S., Miettinen, J.J., Bewicke-Copley, F., Parsons, A., Heckman, C.A., Swanton, C., et al. (2022). CKS1 inhibition depletes leukemic stem cells and protects healthy hematopoietic stem cells in acute myeloid leukemia. Sci. Transl. Med. *14*, eabn3248. https://doi.org/10.1126/scitranslmed.abn3248.

36. Shen, Q., Li, J., Zhang, C., Pan, X., Li, Y., Zhang, X., En, G., and Pang, B. (2023). Pan-cancer analysis and experimental validation identify ndc1 as a potential immunological, prognostic and therapeutic biomarker in pancreatic cancer. Aging (Albany, NY) *15*, 9779–9796. https://doi.org/10.18632/aging.205048.

37. Liu, Q., Gu, L., Qiu, J., and Qian, J. (2023). Elevated NDC1 expression predicts poor prognosis and correlates with immunity in hepatocellular carcinoma. J. Gastrointest. Oncol. *14*, 245–264. https://doi.org/10.21037/jgo-22-1166.

38. Qiao, W., Han, Y., Jin, W., Tian, M., Chen, P., Min, J., Hu, H., Xu, B., Zhu, W., Xiong, L., et al. (2016). Overexpression and biological function of TMEM48 in non-small cell lung carcinoma. Tumour Biol. *37*, 2575–2586. https://doi.org/10.1007/s13277-015-4014-x.

39. Akkafa, F., Koyuncu, İ., Temiz, E., Dagli, H., Dïlmec, F., and Akbas, H. (2018). miRNA-mediated apoptosis activation through TMEM 48 inhibition in A549 cell line. Biochem. Biophys. Res. Commun. *503*, 323–329. https://doi.org/10.1016/j.bbrc.2018.06.023.

40. Yeh, H.W., Lee, S.S., Chang, C.Y., Lang, Y.D., and Jou, Y.S. (2019). A new switch for TGFbeta in cancer. Cancer Res. *79*, 3797–3805. https://doi.org/10.1158/0008-5472.CAN-18-2019.

41. Lang, Y.D., and Jou, Y.S. (2020). PSPC1: a contextual determinant of tumor progression. Mol. Cell. Oncol. *7*, 1721253. https://doi.org/10.1080/23723556.2020.1721253.

42. Cai, S.F., and Levine, R.L. (2019). Genetic and epigenetic determinants of AML pathogenesis. Semin. Hematol. *56*, 84–89. https://doi.org/10.1053/j.seminhematol.2018.08.001.

43. Guallar, D., Bi, X., Pardavila, J.A., Huang, X., Saenz, C., Shi, X., Zhou, H., Faiola, F., Ding, J., Haruehanroengra, P., et al. (2018). RNA-dependent chromatin targeting of TET2 for endogenous retrovirus control in pluripotent stem cells. Nat. Genet. *50*, 443–451. https://doi.org/10.1038/s41588-018-0060-9.

44. Yan, H., Wang, Z., Sun, Y., Hu, L., and Bu, P. (2021). Cytoplasmic NEAT1 suppresses AML stem cell self-renewal and leukemogenesis through inactivation of Wnt signaling. Adv. Sci. (Weinh) *8*, e2100914. https://doi.org/10.1002/advs.202100914.

45. Zhao, C., Wang, S., Zhao, Y., Du, F., Wang, W., Lv, P., and Qi, L. (2019). Long noncoding RNA NEAT1 modulates cell proliferation and apoptosis by regulating miR-23a-3p/SMC1A in acute myeloid leukemia. J. Cell. Physiol. *234*, 6161–6172. https://doi.org/10.1002/jcp.27393.

46. Hsing, M., Wang, Y., Rennie, P.S., Cox, M.E., and Cherkasov, A. (2020). ETS transcription factors as emerging drug targets in cancer. Med. Res. Rev. *40*, 413–430. https://doi.org/10.1002/med.21575.

47. Huang, H.H., Chen, F.Y., Chou, W.C., Hou, H.A., Ko, B.S., Lin, C.T., Tang, J.L., Li, C.C., Yao, M., Tsay, W., et al. (2019). Long non-coding RNA HOXB-AS3 promotes myeloid cell proliferation and its higher expression is an adverse prognostic marker in patients with acute myeloid leukemia and myelodysplastic syndrome. BMC Cancer *19*, 617. https://doi.org/10.1186/s12885-019-5822-y.

48. de Jonge, H.J., Woolthuis, C.M., Vos, A.Z., Mulder, A., van den Berg, E., Kluin, P.M., van der Weide, K., de Bont, E.S., Huls, G., Vellenga, E., and Schuringa, J.J. (2011). Gene expression profiling in the leukemic stem cell-enriched CD34+ fraction identifies target genes that predict prognosis in normal karyotype AML. Leukemia *25*, 1825–1833. https://doi.org/10.1038/leu.2011.172.

49. Stewart, S.A., Dykxhoorn, D.M., Palliser, D., Mizuno, H., Yu, E.Y., An, D.S., Sabatini, D.M., Chen, I.S.Y., Hahn, W.C., Sharp, P.A., et al. (2003). Lentivirus-delivered stable gene silencing by RNAi in primary cells. RNA *9*, 493–501. https://doi.org/10.1261/rna.2192803.

50. Stringer, B.W., Day, B.W., D'Souza, R.C.J., Jamieson, P.R., Ensbey, K.S., Bruce, Z.C., Lim, Y.C., Goasdoué, K., Offenhäuser, C., Akgül, S., et al. (2019). A reference collection of patient-derived cell line and xenograft models of proneural, classical and mesenchymal glioblastoma. Sci. Rep. *9*, 4902. https://doi.org/10.1038/s41598-019-41277-z.

51. Holst, J., Szymczak-Workman, A.L., Vignali, K.M., Burton, A.R., Workman, C.J., and Vignali, D.A.A. (2006). Generation of T-cell receptor retrogenic mice. Nat. Protoc. *1*, 406–417. https://doi.org/10.1038/nprot.2006.61.

52. Saito, Y., Chapple, R.H., Lin, A., Kitano, A., and Nakada, D. (2015). AMPK protects leukemia-initiating cells in myeloid leukemias from metabolic stress in the bone marrow. Cell Stem Cell *17*, 585–596. https://doi.org/10.1016/j.stem.2015.08.019.

53. Naviaux, R.K., Costanzi, E., Haas, M., and Verma, I.M. (1996). The pCL vector system: rapid production of helper-free, high-titer, recombinant retroviruses. J. Virol. *70*, 5701–5705. https://doi.org/10.1128/JVI.70.8.5701-5705.1996.

54. Campeau, E., Ruhl, V.E., Rodier, F., Smith, C.L., Rahmberg, B.L., Fuss, J.O., Campisi, J., Yaswen, P., Cooper, P.K., and Kaufman, P.D. (2009). A versatile viral system for expression and depletion of proteins in mammalian cells. PLoS One *4*, e6529. https://doi.org/10.1371/journal.pone.0006529.

55. Dobin, A., Davis, C.A., Schlesinger, F., Drenkow, J., Zaleski, C., Jha, S., Batut, P., Chaisson, M., and Gingeras, T.R. (2013). STAR: ultrafast universal RNA-seq aligner. Bioinformatics *29*, 15–21. https://doi.org/10.1093/bioinformatics/bts635.

56. Anders, S., Pyl, P.T., and Huber, W. (2015). HTSeq–a Python framework to work with high-throughput sequencing data. Bioinformatics *31*, 166–169. https://doi.org/10.1093/bioinformatics/btu638.

57. Love, M.I., Huber, W., and Anders, S. (2014). Moderated estimation of fold change and dispersion for RNA-seq data with DESeq2. Genome Biol. *15*, 550. https://doi.org/10.1186/s13059-014-0550-8.

58. Subramanian, A., Tamayo, P., Mootha, V.K., Mukherjee, S., Ebert, B.L., Gillette, M.A., Paulovich, A., Pomeroy, S.L., Golub, T.R., Lander, E.S., and Mesirov, J.P. (2005). Gene set enrichment analysis: a knowledge-based approach for interpreting genome-wide expression profiles. Proc. Natl. Acad. Sci. USA *102*, 15545–15550. https://doi.org/10.1073/pnas.0506580102.

59. Langmead, B., and Salzberg, S.L. (2012). Fast gapped-read alignment with Bowtie 2. Nat. Methods *9*, 357–359. https://doi.org/10.1038/nmeth.1923.

60. Li, H., Handsaker, B., Wysoker, A., Fennell, T., Ruan, J., Homer, N., Marth, G., Abecasis, G., and Durbin, R.; 1000 Genome Project Data Processing Subgroup (2009). The Sequence Alignment/Map format and SAMtools. Bioinformatics *25*, 2078–2079. https://doi.org/10.1093/bioinformatics/btp352.

61. Tarasov, A., Vilella, A.J., Cuppen, E., Nijman, I.J., and Prins, P. (2015). Sambamba: fast processing of NGS alignment formats. Bioinformatics *31*, 2032–2034. https://doi.org/10.1093/bioinformatics/btv098.

62. Ramírez, F., Dündar, F., Diehl, S., Grüning, B.A., and Manke, T. (2014). deepTools: a flexible platform for exploring deep-sequencing data. Nucleic Acids Res. *42*, W187–W191. https://doi.org/10.1093/nar/gku365.

63. Yu, G., Wang, L.G., and He, Q.Y. (2015). ChIPseeker: an R/Bioconductor package for ChIP peak annotation, comparison and visualization. Bioinformatics *31*, 2382–2383. https://doi.org/10.1093/bioinformatics/btv145.

64. Heinz, S., Benner, C., Spann, N., Bertolino, E., Lin, Y.C., Laslo, P., Cheng, J.X., Murre, C., Singh, H., and Glass, C.K. (2010). Simple combinations of lineage-determining transcription factors prime cis-regulatory elements required for macrophage and B cell identities. Mol. Cell *38*, 576–589. https://doi.org/10.1016/j.molcel.2010.05.004.

65. Feng, J., Liu, T., Qin, B., Zhang, Y., and Liu, X.S. (2012). Identifying ChIP-seq enrichment using MACS. Nat. Protoc. *7*, 1728–1740. https://doi.org/10.1038/nprot.2012.101.

66. Zhu, G., Luo, H., Feng, Y., Guryanova, O.A., Xu, J., Chen, S., Lai, Q., Sharma, A., Xu, B., Zhao, Z., et al. (2021). HOXBLINC long non-coding RNA activation promotes leukemogenesis in NPM1-mutant acute myeloid leukemia. Nat. Commun. *12*, 1956. https://doi.org/10.1038/s41467-021-22095-2.

67. Li, S.L., Schlegel, W., Valente, A.J., and Clark, R.A. (1999). Critical flanking sequences of PU.1 binding sites in myeloid-specific promoters. J. Biol. Chem. *274*, 32453–32460. https://doi.org/10.1074/jbc.274.45.32453.

68. Bottomly, D., Long, N., Schultz, A.R., Kurtz, S.E., Tognon, C.E., Johnson, K., Abel, M., Agarwal, A., Avaylon, S., Benton, E., et al. (2022). Integrative analysis of drug response and clinical outcome in acute myeloid leukemia. Cancer Cell *40*, 850–864.e9. https://doi.org/10.1016/j.ccell.2022.07.002.

STAR★METHODS

KEY RESOURCES TABLE

REAGENT or RESOURCE	SOURCE	IDENTIFIER
Antibodies		
PSPC1	Santa Cruz Biotechnology	Cat#sc-374181; RRID:AB_10989076
PSPC1	Bethyl Laboratories	Cat# A303-206A; RRID:AB_10954256
β-Actin	Cell Signaling Technology	Cat#3700; RRID:AB_2242334
PU.1	Abcam	Cat# ab302623
Phospho-Rpb1 CTD (Ser5)	Cell Signaling Technology	Cat#13523; RRID:AB_2798246
IgG	Bethyl Laboratories	Cat#P120-101; RRID:AB_479829
NONO	Santa Cruz Biotechnology	Cat#sc-166702; RRID:AB_2152178
NONO	Santa Cruz Biotechnology	Cat#sc-376865; RRID:AB_2828025
SFPQ	Proteintech	Cat#15585-1-AP; RRID:AB_10697653
ERG	Proteintech	Cat#14356-1-AP; RRID:AB_2098423
ETS1	Proteintech	Cat#12118-1-AP; RRID:AB_10664925
GABPA	Proteintech	Cat#21542-1-AP; RRID:AB_10858481
FLI1	Cell Signaling Technology	Cat#35980; RRID:AB_2799091
RUNX1	Santa Cruz Biotechnology	Cat# sc-365644; RRID:AB_10843207
NDC1	Novus Biologicals	Cat# NBP1-91603; RRID:AB_11030742
MCM7	Cell Signaling Technology	Cat#3735; RRID:AB_2142705
HAUS8	Novus Biologicals	Cat# NBP2-42849; RRID:AB_2665500
CKS1	Invitrogen	Cat# 36-6800; RRID:AB_2533274
CDCA25	Proteintech	Cat#67418-1-Ig; RRID:AB_2882658
Anti-mouse Lineage cocktail APC	BD Biosciences	Cat#5508074; RRID:AB_1645213
Anti-mouse Sca-1 PE-Cy7	BD Biosciences	Cat#558162; RRID:AB_647253
Anti-mouse c-kit (CD117) PerCp-Cy5.5	BD Biosciences	Cat#560557; RRID:AB_1645258
Anti-mouse CD34 Alexa Fluor 700	BD Biosciences	Cat#560518; RRID:AB_1727471
Anti-mouse CD16/32 APC-Cy7	BioLegend	Cat#101327; RRID:AB_2104158
Anti-mouse CD135 BV421	BD Biosciences	Cat#562898; RRID:AB_2737876
Anti-mouse Gr-1 PerCP-Cy5.5	BD Biosciences	Cat#552093; RRID:AB_394334
Anti-mouse Mac-1 PE	BD Biosciences	Cat#553311; RRID:AB_394775
Anti-mouse c-kit APC	BD Biosciences	Cat#553356; RRID:AB_398536
Anti-mouse CD8a PE	BD Biosciences	Cat#553033; RRID:AB_394571
Anti-mouse CD4 PerCP-Cy5.5	BD Biosciences	Cat#550954; RRID:AB_393977
Anti-mouse IgM PE-Cy7	BD Biosciences	Cat#552867; RRID:AB_394500
Anti-mouse B220 APC	BD Biosciences	Cat#553092; RRID:AB_398531
Anti-mouse Ter119 APC	BD Biosciences	Cat#557909; RRID:AB_398635
Anti-mouse CD71 PE	BD Biosciences	Cat#553267; RRID:AB_394744
Anti-mouse CD45.1 FITC	BD Biosciences	Cat#553775; RRID:AB_395043
Anti-mouse CD45.2 PerCP-Cy5.5	BD Biosciences	Cat#552950; RRID:AB_394528
Anti-human CD45 BV421	BD Biosciences	Cat#563879; RRID:AB_2744402
Anti-human CD33 PE	BD Biosciences	Cat#555450; RRID:AB_395843
Anti-human CD11b BV421	BioLegend	Cat#301324; RRID:AB_10933087
Anti-human CD235a APC	BD Biosciences	Cat#551336; RRID:AB_398499
Chemicals, peptides, and recombinant proteins		
Recombinant Human SCF	Peprotech	Cat#300-07
Recombinant Human GM-CSF	Peprotech	Cat#300-03
Recombinant Human IL-3	Peprotech	Cat#200-03

(*Continued on next page*)

Continued

REAGENT or RESOURCE	SOURCE	IDENTIFIER
Recombinant Human IL-6	Peprotech	Cat#200-06
Recombinant mouse SCF	Peprotech	Cat#250-03
Recombinant mouse FLT3 Ligand	Peprotech	Cat#300-19
Recombinant mouse TPO	Peprotech	Cat#315-14
Recombinant mouse IL-3	Peprotech	Cat#213-13
Puromycin	Thermo Fisher Scientific	Cat# A1113803
Polybrene	Sigma-Aldrich	Cat# TR-1003-G
pI:pC	InvivoGen	Cat# vac-pic
Critical commercial assays		
High Capacity cDNA Reverse Transcription Kit	Thermo Fisher Scientific	Cat#4368814
KAPA Stranded mRNA-Seq Kit	Roche	Cat#KK8421
MicroPlex Library Preparation Kit	Diagenode	Cat#C05010001
Lineage Cell Depletion Kit, mouse	Miltenyi Biotec	Cat#130-110-470
CD117 MicroBeads, mouse	Miltenyi Biotec	Cat#130-097-146
CD45 MicroBeads, human	Miltenyi Biotec	Cat#130-045-801
Deposited data		
RNA-seq	This study	GEO: GSE247301
ChIP-seq	This study	GEO: GSE247300
Microarray data	Huang et al.[47]; de jonge et al.,[48]	GEO: GSE114868, GEO: GSE30029
Epigenomics Studies in Acute Myeloid Leukemia (AML)	The Database of Genotypes and Phenotypes (dbGAP)	dbGAP: phs001027
Experimental models: Cell lines		
LentiX-293T	TAKARA	Cat#632180; RRID:CVCL_4401
MOLM13	DSMZ	Cat#ACC 554; RRID:CVCL_2119
MONO-MAC1	DSMZ	Cat#ACC 252; RRID:CVCL_1425
NOMO1	DSMZ	Cat#ACC 542; RRID:CVCL_1609
THP1	ATCC	Cat#TIB-202; RRID:CVCL_0006
EOL1	DSMZ	Cat#ACC 386; RRID:CVCL_0258
OCI-AML3	DSMZ	Cat#ACC 582; RRID:CVCL_1844
OCI-AML5	DSMZ	Cat#ACC 247; RRID:CVCL_1620
TF1	DSMZ	Cat#ACC 334; RRID:CVCL_0559
Experimental models: Organisms/strains		
NOD.Cg-*Prkdc*^{scid} *IL2rg*^{null} (NSG) mouse	Jackson Laboratory	Strain #:005557; RRID:IMSR_JAX:005557
NOD/ShiLtJGpt-*Prkdc*^{em26Cd52}*Il2rg*^{em26Cd22} Rosa26$^{em1Cin(hCSF2\&IL3\&KITLG)}$/GptCrl (NCG-M) mouse	Charles River	Strain #: 715
C57BL/6J mouse	Jackson Laboratory	Strain #:000664; RRID:IMSR_JAX:000664
B6.SJL-*Ptprc*^{a} *Pepc*^{b}/BoyJ mouse	Jackson Laboratory	Strain #:002014; RRID:IMSR_JAX:002014
Pspc1$^{f/f}$	From Dr. Peter Tontonoz	N/A
Mx1-Cre	Jackson Laboratory	Strain #:003556; RRID:IMSR_JAX:003556
Oligonucleotides		
For primers, see Table S2	N/A	N/A
Recombinant DNA		
pLKO.1 puro	Stewart et al.[49]	Cat#8453; RRID:Addgene_8453
pLKO.1-shPSPC1-2	This study	N/A
pLKO.1-shPSPC1-4	This study	N/A
pLKO.1-shNONO-1	This study	N/A
pLKO.1-shNONO-2	This study	N/A
pLKO.1-shPU.1-1	This study	N/A

(*Continued on next page*)

Continued

REAGENT or RESOURCE	SOURCE	IDENTIFIER
pLKO.1-shPU.1-2	This study	N/A
pLKO.1-shNDC1-4	This study	N/A
pLKO.1-shNDC1-7	This study	N/A
pLKO.1-shPspc1-a	This study	N/A
pLKO.1-shPspc1-b	This study	N/A
LentiCRISPRv2	Stringer et al.[50]	Cat#98290; RRID:Addgene_98290
pMSCV-IRES-GFP II	Holst et al.[51]	Cat#52107; RRID:Addgene_52107
pMSCV-Pspc1-IRES-GFP	This study	N/A
pMSCV-MLL-AF9-IRES-GFP	Saito et al.[52]	Cat#71443; RRID:Addgene_71443
pCL-Eco	Naviaux et al.[53]	Cat#12371; RRID:Addgene_12371
pLenti-GFP	Campeau et al.[54]	Cat#17446; RRID:Addgene_17446
pLenti-PSPC1 FL, shRNA-resistant	This study	N/A
pLenti-PSPC1 ΔRRM	This study	N/A
Software and algorithms		
GraphPad Prism 10	GraphPad software	https://www.graphpad.com/
Flowjo Software (version 10.9.0)	Flowjo	https://www.flowjo.com/
R	N/A	https://www.r-project.org/
trim_galore(v 0.6.7)	N/A	https://github.com/FelixKrueger/TrimGalore
STAR(v 2.7.10a)	Dobin et al.[55]	https://github.com/alexdobin/STAR
HTSeq(v 2.0.2)	Anders et al.[56]	https://htseq.readthedocs.io/en/latest/index.html
DESeq2(v 1.36.0)	Love et al.[57]	https://bioconductor.org/packages/release/bioc/html/DESeq2.html
GSEA(v 3.0)	Subramanian et al.[58]	https://www.gsea-msigdb.org/gsea/index.jsp
bowtie2(v 2.4.5)	Langmead and Salzberg[59]	https://bowtie-bio.sourceforge.net/bowtie2/index.shtml
SAMtools (v1.15.1)	Li et al.[60]	https://github.com/samtools/samtools
Sambamba (v 0.8.2)	Tarasov et al.[61]	https://lomereiter.github.io/sambamba/
DeepTools (v 3.5.1)	Ramirez et al.[62]	https://deeptools.readthedocs.io/en/develop/#
ChIPseeker(v 1.32.1)	Yu et al.[63]	https://bioconductor.org/packages/release/bioc/html/ChIPseeker.html
homer(v 4.11)	Heinz et al.[64]	http://homer.ucsd.edu/homer/
MACS2 (v 2.2.7.1)	Feng et al.[65]	https://github.com/macs3-project/MACS

EXPERIMENTAL MODEL AND STUDY PARTICIPANT DETAILS

Human patient samples and primary cell culture

Human primary AML patient samples were collected at the time of diagnosis, relapse, or remission after written informed consent at City of Hope Hospital or MD Anderson Cancer Center in congruence with the protocol approved by the institutional review board (IRB). Characteristics of the AML patients are provided in Table S3. The leukemic samples were cryopreserved in liquid nitrogen until used. AML #2017-129, #2016-35, #6407 cells were cultured in IMDM medium (Gibco) supplemented with 20% FBS, 10 ng/mL of hSCF, mTPO, mFLT3, hIL3, hIL-6, and 1% P/S. AML #676 and #6303 cells were cultured in StemSpan™ SFEM II (Stem Cell Technologies) supplemented with 10 ng/mL of hSCF, mTPO, mFLT3, hIL3, hIL-6, 35nM UM171, and 500nM Stem regenin1 (SR1), and 1% P/S. $CD34^+$ normal HSPCs were purchased from Lonza and Stem Cell Technologies and cultured in IMDM containing 20% FBS, 100 ng/mL of hSCF and mTPO, 10 ng/mL of mFLT3, 20 ng/mL of hIL6, and 1% P/S. All the cytokines were purchased from Peprotech.

Mice

C57BL/6J (CD45.2) background *Pspc1*$^{f/f}$ and Mx1-cre mice were obtained from Dr. Peter Tontonoz (University of California Los Angeles) and the Jackson Laboratory, respectively. Mx1-cre-induced gene deletion was achieved by intraperitoneal injection of *pI:pC* (10 mg/kg; InvivoGen) three times every other day. The genotyping PCR primers are listed in Table S2. B6.SJL (BoyJ, CD45.1) and NOD.Cg-*Prkdc*^{scid}*IL2rg*^{null} (NSG) mice were purchased from the Jackson Laboratory, and NOD/ShiLtJGpt-*Prkdc*^{em26Cd52}*Il2rg*^{em26Cd22}Rosa26$^{em1Cin(hCSF2\&IL3\&KITLG)}$/GptCrl (NCG-M) mice were purchased from Charles River. Both male and female mice were used for experiments with age- and gender-matched littermates as control. All animal studies were performed with approval

from the University of Texas Health Science Center at San Antonio Institutional Animal Care and Use Committee and conducted following institutional and national regulatory standards.

Cell lines

MOLM13, NOMO1, THP1, and EOL1 cells were cultured in RPMI 1640 medium (Sigma-Aldrich) containing 10% FBS (Gibco) and 1% Penicillin-Streptomycin (P/S) (Gibco). TF-1 cells were kept in RPMI 1640 with 10% FBS, 1% P/S, and 2 ng/mL hGM-CSF. MONO-MAC1 cells were maintained in RPMI 1640 with 10% FBS, 1% P/S, 2mM L-Glutamine (Gibco), 1X Non-Essential Amino Acid (Gibco), and 1mM sodium pyruvate (Gibco). OCI-AML3 cells were cultured in α-MEM medium (Corning) with 20% FBS, 1% P/S, and 10 ng/mL hGM-CSF was added for OCI-AML5 cells. HEK293T cells were maintained in DMEM medium (Sigma-Aldrich) containing 10% FBS and 1% P/S. All the cells were incubated at 37°C with 5% CO_2 and routinely tested for mycoplasma contamination (InvivoGen).

METHOD DETAILS

Plasmids

The shRNA-resistant PSPC1 full-length plasmid was generated by introducing silent mutations at shRNA target site and purchased from Vector Builder and deletion constructs were subcloned by mutagenesis (NEB). The shRNAs targeting human PSPC1 (#2: TRCN0000154409; #4: TRCN0000154860), PU.1 (#1: TRCN0000426240; #2: TRCN0000020534) were purchased from Sigma-Aldrich. *NDC1*-targeting shRNA expressing vectors (#4: CGCACTTAGTAGCAGCATCAT; #7: GGTAACAGTGCAGCAATATTC) were cloned in pLKO.1-puro plasmid (Addgene, #8453). The lentiviral vectors co-expressing Cas9 and sgRNA against PSPC1 were generated based on the pLentiCRISPRv2-puro plasmid (Addgene, #98290). Sense and anti-sense oligos were annealed using primers listed in Table S2 and then ligated into pLentiCRISPRv2-puro plasmid digested with BsmBI. pMSCV-IRES-GFP empty vector (#52107) and pMSCV-MLL-AF9-IRES-GFP was purchased from Addgene (#71443) while pMSCV-Pspc1-IRES-GFP vector was purchased from Vector Builder.

Lentivirus production and generation of stable cell lines

Lentiviral particles for overexpression or knockdown plasmids were produced in HEK293T cells transfected with packaging (psPAX2) and envelope (VSV-G) plasmids using Lipofectamine 3000 (Invitrogen). The lentiviral supernatants were harvested twice at 24- and 48-hour time points after transfection, passed through a membrane filter with 0.45 μm pore size, and concentrated with a Lenti-X concentrator (Takara, #631232). Host cells were infected with the lentiviral particles in the presence of 8 μg/mL polybrene (Sigma-Aldrich, #TR-1003-G), then selected using 1 μg/mL puromycin (Gibco, #A1113803) or sorted for GFP^+ cells.

Retrovirus preparation and *in vitro* colony-forming assay

Retroviruses were produced in 293T cells by transfecting retroviral construct and pCL-Eco with Lipofectamine 3000. Virus particles were harvested twice at 24- and 48-hour points before concentration. Bone marrow (BM) cells were collected from 8-10 weeks wild-type or *Pspc1* KO mice, and LK ($Lin^-c\text{-}kit^+$) cells were enriched with the Mouse Lineage Cell Depletion Kit (Miltenyi Biotec, #130-110-470) and mouse CD117 MicroBead Kit (Miltenyi Biotec, #131-091-224). BM progenitor cells were then transduced with retroviruses by two rounds of spinoculation in the presence of 8 μg/mL polybrene. Forty-eight hours after transduction, cells were plated in methylcellulose medium (STEMCELL Technologies, #MethoCult M3134) supplemented with 100 ng/mL mSCF, 10 ng/mL mIL-3, 50 ng/mL mTPO, 10 ng/mL mGM-CSF, 4U/mL hEPO, 50 ng/mL hIL-6. All the cytokines used were purchased from Peprotech. Cultures were incubated at 37°C with 5% CO_2, and the colonies were counted on day 7. Serial replating was then performed by collecting colony cells and replating them into new dishes with methylcellulose medium every 7 days.

Bone marrow transplantation (BMT)

For primary BMT, $Lin^-c\text{-}kit^+$ cells were isolated from 8-10 weeks mice (CD45.2) according to the aforementioned strategies and transduced with retroviruses in the presence of 8 μg/mL polybrene by two rounds of spinoculation. Cells were then resuspended in PBS containing 2% FBS and transplanted via tail vein injection into lethally (800 cGy) irradiated 8- to 10-week-old BoyJ (CD45.1) recipient mice. For each recipient mouse, $1x10^6$ donor cells and $5x10^5$ radioprotective helper cells from BoyJ (CD45.1) mice were transplanted. For limiting dilution assay, GFP^+ BM cells were sorted from primary BMT mice (3 mice/group) and transplanted into sublethally (550 cGy) irradiated BoyJ recipient mice with three different doses of donor cells for each group. ELDA software was used to analyze the frequency of leukemia stem cells. When needed, recipient mice were injected with *pI:pC* intraperitoneally three times 13 days after transplantation. Leukemic mice were sacrificed when they became moribund or showed signs of illness. Peripheral blood (PB), spleen, liver, femur, and tibia were collected at the time of sacrifice. BM cytospin and blood smear slides were stained with Wright-Giemsa. Portions of the spleen, liver, and femur were subject to hematoxylin and eosin (H&E) staining.

Competitive repopulation assay

$5x10^5$ 8-week-old BoyJ (CD45.1) whole bone marrow (BM) cells were mixed with either $5x10^5$ 8-week-old $Pspc1^{f/f}$ or $Pspc1^{f/f}$;Mx1-cre (CD45.2) BM cells and injected into lethally irradiated BoyJ recipient mice via tail vein injection. One month after the transplantation, *pI*:pC (10mg/kg) was injected in the recipient mice three times to induce *Pspc1* gene deletion. Peripheral Blood (PB) was collected monthly to monitor the chimerism by examining the percentage of CD45.1 and CD45.2 over 5 months after *pI:pC* injection.

Xenotransplantation assay

AML patient cells were transduced with lentivirus carrying shPSPC1 or shControl in the presence of 8 μg/mL polybrene. Twenty-four hours later, infected cells were selected by 1 μg/mL puromycin for 2 days, and then 1-2x10^6 cells were transplanted into sublethally irradiated NSG (250 cGy) or NCG-M (200 cGy) mice. MOLM13 and OCI-AML5 cells were transduced with lentiviruses and selected by 1 μg/mL puromycin for 2 days. 1x10^6 cells (for MOLM13) or 2x10^6 cells (for OCI-AML5) were transplanted into sublethally irradiated NSG mice. Recipient mice were monitored to assess AML burden.

In vivo homing assay

For the homing experiment, 5x10^6 MOLM13 cells transduced with shControl, shPSPC1-2, or shPSPC1-4 lentivirus were transplanted into NSG mice via tail-vein injection. Homing of the AML cells in the BM was assessed at 16 hours after transplantation by flow cytometry.

Flow cytometry

Flow cytometric analysis of mouse BM cells was performed as previously described.[66] Briefly, for HSPC cells, BM cells were stained with APC-anti-Lineage cocktail (BD Biosciences, #5508074), PE-Cy7-anti-Sca1 (BD Biosciences, #558162), PerCP-Cy5.5-anti-c-kit (BD Biosciences, #560557), Alexa Flour 700-anti-CD34 (BD Biosciences, #560518), APC-Cy7-anti-CD16/32 (BioLegend, #101327), BV421-anti-CD135 (BD Biosciences, #562898). For analysis of mature cells, BM, PB, and spleen cells were stained with PerCP-Cy5.5-anti-Gr-1(BD Biosciences, #552093), PE-anti-Mac-1 (BD Biosciences, #553311), APC-anti-c-kit (BD Biosciences, #553356), PE-anti-CD8a (BD Biosciences, #553033), PerCP-Cy5.5-anti-CD4 (BD Biosciences, #550954), PE-Cy7-anti-IgM (BD Biosciences, #552867), APC-anti-B220 (BD Biosciences, #553092), APC-anti-Ter119 (BD Biosciences, #557909), and PE-anti-CD71 (BD Biosciences, #553267). To distinguish CD45.2 donor-derived cells from recipient CD45.1 mice, PerCP-Cy5.5-anti-CD45.2 (BD Biosciences, #552950) and FITC-anti-CD45.1 (BD Biosciences, #553775) were added. Leukemia cells from NSG mice were stained with BV421-anti-hCD45 (BD Biosciences, #563879) and PE-anti-hCD33 (BD Biosciences, #555450) to analyze the frequency of tumor engraftment.

For cell cycle analysis, cells were stained with Propidium Iodide solution (BioLegend, #421301) after fixation with 70% EtOH. To analyze apoptosis, cells were stained with BV421-Annexin V (BioLegend, #640924) and 7-AAD (BioLegend, #420404) in Annexin V binding buffer (BD Biosciences, #556454). Differentiation assay was analyzed by staining cells with BV421-anti-hCD11b (BioLegend, #301324) or APC-anti-hCD235a (BD Biosciences, #551336). All flow cytometric analysis was performed on the BD FACSCelesta, and the data were analyzed with FlowJo software.

Western blots and co-immunoprecipitation (co-IP) assay

Cells were lysed with either RIPA lysis buffer (Millipore, #20-188) or IP lysis buffer (Thermo Scientific, #87788), supplemented with 1× protease inhibitor (Sigma-Aldrich, #S8830) for 15 minutes on ice. Immunoblotting was performed with the following antibodies: anti-PSPC1 (Santa Cruz, #sc-374181), anti-NONO (Santa Cruz, #sc-166702), anti-PU.1 (Abcam, #ab302623), anti-NDC1 (Novus Biologicals, #NBP1-91603), anti-MCM7 (Cell Signaling, #3735), anti-HAUS8 (Novus Biologicals, #NBP2-42849), anti-CDCA5 (Proteintech, #67418-1-Ig), anti-CKS1 (Invitrogen, #36-6800), and anti-β-Actin (Cell Signaling, #3700). For co-IP assay, cells were lysed with IP lysis buffer, followed by mild sonication. Lysates were incubated with anti-PSPC1 (Bethyl Laboratories, #A303-206A) or anti-PU.1 (Abcam, #ab302623) overnight at 4°C. After washing the beads four times with IP lysis buffer, the bound proteins were analyzed by western blotting with the following antibodies: anti-PU.1 (Abcam, #ab302623), anti-PSPC1 (Santa Cruz, #sc-374181), anti-ERG (Proteintech, #14356-1-AP), anti-ETS1 (Proteintech, #12118-1-AP), anti-GABPA (Proteintech, #21542-1-AP), anti-FLI1 (Cell signaling, #35980), and anti-RUNX1 (Santa Cruz, #sc-365644).

Immunofluorescence (IF) assay

Cells were resuspended in PBS and incubated on a fibronectin-coated coverslip in a 6-well plate at RT to enable the cells to attach. 30 min later, non-attached cells were removed by aspirating PBS. Cells were then fixed with 3.7% formaldehyde for 10 min, permeabilized by 0.5% Triton X-100 for 10 min, and blocked with PBS supplemented with 0.5% BSA for 1 hr. After incubation with primary antibodies [anti-NONO (Santa Cruz, #sc-376865), anti-SFPQ (Proteintech, #15585-1-AP), and anti-PSPC1 (Cell Signaling, #65992)] at 4°C for overnight, cells were washed with PBS three times and incubated with Alexa Fluor 488 anti-rabbit secondary antibody (Invitrogen, #A11034) and Alexa Fluor 594 anti-mouse secondary antibody (Invitrogen, #A11032) at RT for 1 hr. After washing with PBS three times, cells were mounted with a DAPI-containing medium (Vector Laboratories, #H-1200). Immunofluorescence images were captured using a confocal microscope (Carl Zeiss, LSM710).

Luciferase assay

Previously reported PU.1 binding motif sequence was cloned into pNL1.1 empty vector (Promega, USA) by mutagenesis to generate a pNL1.1-PU.1 motif plasmid.[67] OCI-AML5 cells were transduced with shRNA targeting PU.1, PSPC1, or control. Twenty-four hours post-infection, cells were transfected with pNL1.1-PU.1 motif vector with pTK-firefly vector (Promega). pTK-firefly vector was used to normalize the nluc luciferase activity. Forty-eight hours later, cells were prepared for luciferase assay using a Nano-glo dual luciferase assay system (Promega) following the manufacturer's protocol. Luciferase activity was determined by relative light unit (RLU) using the Varioskan LUX microplate reader (Thermo Fisher).

RNA extraction and quantitative reverse transcription PCR (RT-qPCR)

Total RNAs were isolated using TRIzol Reagent (Invitrogen, #15596026). 1-2 μg of RNAs were reverse transcribed into cDNA using the High-Capacity cDNA Reverse Transcription Kit (Applied Biosystems, #4368814) and subject to qPCR reactions was performed in the Applied Biosystems QuantStudio3 with the Fast SYBR Green Master Mix (Applied Biosystems, #4385612). Levels of tested transcripts were determined with the $2^{-\Delta\Delta Ct}$ method and normalized to the expression of *ACTB*, which serves as the internal control. The primers used in RT-qPCR were listed in Table S2.

RNA-seq and data analysis

Total RNA was extracted using TRIzol Reagent. 1-2 μg of total RNAs were consumed to construct the mRNA-seq libraries using the KAPA-stranded mRNA-seq kit. Each library was quantified using a Qubit fluorometer (Thermo Fisher Scientific), and the size distribution was assessed using a Bioanalyzer (Agilent Technologies). All samples were sequenced with the mode of paired-end 150 bp on the Illumina Novaseq 6000 platform.

The raw data was trimmed by trim_galore(v 0.6.7) with the parameter of –paired -q 25 –phred33 –length 35 -e 0.1 –stringency 2. The clean reads were aligned to the human genome(GRCh38) using STAR(v 2.7.10a)[55] and then HTSeq(v 2.0.2)[56] was used to calculate the raw read counts for each gene within the GTF file and each sample. The count matrix was used to identify differentially expressed genes(DEGs) by DESeq2(v 1.36.0)[57] with the cutoff of FDR < 0.05 and |Fold change| >1. Transcripts per million(TPM, transformed from raw count value) matrix was used to identify differentially expressed pathways by GSEA.[58]

Beat AML 2.0 is the latest and harmonized data collection of Beat AML with a cumulative cohort of 805 patients (942 specimens).[68] Data can be found at https://biodev.github.io/BeatAML2/. In addition, phs001027 is a dataset from the database of Genotypes and Phenotypes (dbGaP): *Epigenomics studies in Acute Myeloid Leukemia*. This study was designed to understand the molecular basis of disease progression in AML through interrogation of 138 paired (diagnosis and relapse) patient specimens.

Chromatin immunoprecipitation (ChIP)-qPCR and ChIP-seq

ChIP was performed with a dual cross-linking protocol that starts with 2 mM disuccinimidyl glutarate (DSG) (CovaChem, #13301) for 30 minutes, followed by 1% formaldehyde (Sigma-Aldrich) for 10 minutes at RT. Cross-linking was quenched with 0.125 M Glycine for 5 minutes at RT. Nuclei were isolated sequentially using buffers LB1 [50 mM HEPES-KOH (pH 7.5), 140 mM NaCl, 1 mM EDTA (pH 8.0), 10% glycerol, 0.5% NP-40, 0.25% Triton X-100 and 1× protease inhibitor], LB2 [10 mM Tris-HCl (pH 8.0), 200 mM NaCl, 1 mM EDTA (pH 8.0), 0.5 mM EGTA (pH 8.0) and 1× protease inhibitor] and LB3 [10 mM Tris-HCl (pH 8.0), 100 mM NaCl, 1 mM EDTA (pH 8.0), 0.5 mM EGTA (pH 8.0), 0.1% Na-deoxycholate, 0.5% N-lauroylsarcosine and 1× protease inhibitor]. Isolated chromatin was fragmented in Q800R sonicator (QSONICA) and incubated with appropriate amounts of antibodies [5 μg anti-PSPC1 (Bethyl Laboratories, #A303-206A), 2.5 μg anti-PU.1 (Abcam, #ab302623), or 1.5 μg anti-phospho-RPB1 Ser5 (Cell Signaling, #13523)] that have been conjugated to Protein G magnetic beads (Invitrogen) overnight at 4°C. The immunoprecipitates were washed 5 times in RIPA wash buffer [50 mM HEPES-KOH (pH 7.5), 500 mM LiCl, 1 mM EDTA, 1% NP40, 0.7% sodium deoxycholate], twice in 1×TE buffer [10 mM Tris-HCl (pH 8.0) and 1 mM EDTA (pH 8.0)], and finally eluted in the elution buffer [1% SDS, 10 mM Tris-HCl (pH 8.0) and 10 mM EDTA (pH 8.0)]. ChIP'd DNA was reverse cross-linked at 65°C overnight, purified by the treatment with RNase A and proteinase K, and finally subject to either qPCR reactions or ChIP-seq library construction. Primers used for qPCR are listed in Table S2. ChIP-seq libraries were prepared using MicroPlex Library Preparation Kit (Diagenode) and sequenced on Novaseq 6000 with the mode of paired-end 150 bp.

The raw data was trimmed by trim_galore(v 0.6.7) and then the clean reads were aligned to the human genome(GRCh38) using bowtie2(v 2.4.5).[59] The raw SAM files generated by bowtie2 were sorted using SAMtools (v1.15.1)[60] and then PCR duplications were removed by Sambamba (v 0.8.2).[61] Peak calling was performed with MACS2 (v 2.2.7.1)[65] with the parameter of -f BAMPE -g hs -B -q 0.05. DeepTools (v 3.5.1)[62] was used for signal normalization and outputting BigWig file for visualization with options: –normalizeUsing CPM –binSize 50. ChIPseeker(v 1.32.1) was used to annotate peaks and find peak-related genes. Motif prediction was performed using homer(v 4.11)[64] findMotifsGenome.pl.

QUANTIFICATION AND STATISTICAL ANALYSIS

All the experiments were repeated with at least three biological and technical replicates. Results were shown as mean ± standard error of the mean (SEM). Prism software was used to generate graphs and to perform statistical analysis. *P*-values were calculated using a two-tailed unpaired t-test or the appropriate statistical methods as mentioned in the figure legends. Exact *P*-values for each experiment are presented in each figure. ns indicates not significant when the *P*-value is $\geq$ 0.05. Survival durations were analyzed using the Kaplan–Meier method and compared using the log-rank test.